Spinal Response and Injury Association from Whole Body PMHS in the Under Body Blast Loading Environment

By

Christopher J. Dooley

A thesis submitted to Johns Hopkins University in conformity with the requirements for the degree of Master of Science in Mechanical Engineering

Baltimore, Maryland

February, 2016

Abstract

Under body blast (UBB) events deliver extremely high rate vertical loading to the occupants of military vehicles over durations in the range of 2-10 milliseconds. UBB events result in significant, debilitating spinal injuries primarily focused in the thoracolumbar region. To better understand the spinal response in the absence of these injuries, as well as the mechanisms behind spinal injury patterns seen in theater, seven whole body post-mortem human subjects (PMHS) tests were carried out on the Vertically Accelerated Load Transfer System (VALTs) at the Johns Hopkins University Applied Physics Laboratory (APL). Specimens were exposed to relevant UBB conditions, defined by peak velocity and time-to-peak, varying from 4 m/s to 8 m/s on the lower extremity and 4 m/s to 6 m/s on the pelvis. Time-to-peak velocity was in the 5 to 10 ms range. All specimens were similarly positioned based on a comprehensive study documenting anatomical landmarks on seated warfighters. High resolution spinal acceleration and angular velocity data was measured in this unique loading environment with kinetic instrumentation mounted at six locations along the spine from the sacrum to T1.

The objective was to characterize the acceleration and angular velocity response of the PMHS spine in the absence of injury and determine factors that cause injuries when they do occur. Within the seven specimens, three compression fractures, five transverse process fractures, and one iliac wing fracture were sustained. X-ray computed tomography (CT), 3D coordinate measurements, and planar X-ray information were used to define initial conditions. Quantitative CT analysis was utilized to evaluate the multi-level density of each vertebral body in the region of interest for the seven specimens as well as an additional 5 with sustained injuries and revealed a significant difference ($p < 0.05$) in bone mineral density between fractured and non-fractured vertebral bodies.

At a peak input of 222.8 ± 36.9 g in 2 ms at the seat pan, a spine sustained a maximum resultant acceleration at L3 of 93.6 ± 8.9 g, as opposed to at the sacrum acceleration which was

closest to the loading surface. Superior of L3, acceleration peaks decreased monotonically with distance from the seat pan. Minimum relative spinal rotations were observed at the L3-T8 segment, highlighting the axial alignment of the spine over the L3-T8 region with the vertical loading vector. The magnitude of peak acceleration in conjunction with vertical alignment of the spinal column is consistent with mechanisms for compressive spinal injury from the literature; high accelerations of the vertebral body with minimal bending. The confluence of peak acceleration and vertical alignment in the thoracolumbar region also coincides with compressive spinal injury patterns from epidemiological combat injury data, showing spinal injuries from UBB events focused in the L5-T7 region.

Loading severity, spinal alignment, and bone quality all showed influence on vertebral compression fracture in the UBB loading environment. However, each factor was not sufficient to predict fracture in isolation of the other two. Prediction of compressive fracture within the spine may be a function of these three factors combined, and possibly others. Expansion of this research to develop a function for accurate prediction of spinal fracture could facilitate improvements in surrogate design, computational model validity, as well as improved warfighter protection through seat system and vehicle design.

Preface

This research was supported in part by Cooperative Agreements W81XWH-10-2-0065, W81XWH012-0041 (Warrior Injury Assessment Manikin study) and the Department of Veterans Affairs Medical Research. The views expressed in this presentation are those of the authors and do not reflect official policy or position of the Department of the Army, Department of Defense or US Government. No authors are sponsors of this study.

None of this could have been completed without an incredible team and unwavering support. I would like to thank, in no particular order, Kyle Ott and the rest of the VALTS testing team for the tremendous amount of work that goes into producing quality results, Andrew Merkle and Robert Armiger for their leadership and guidance, Dr. Stephen Belkoff and Dr. Liming Voo for their assistance, Dr. Jack Titus for his support in injury identification, and my family and friends for the motivation.

Table of Contents

Abstract i

Preface iii

List of Figures vi

List of Tables ix

1. Introduction 1

2. Spine Anatomy 3

3. Literature Review 7

3.1 Whole Body Testing 8

3.2 Component Level Testing & Injury Mechanisms 9

3.3 Bone Quality Assessment 10

4. Materials and Methods 10

4.1 Test Device 10

4.2 Experimental Input Conditions 12

4.3 Tested Surrogates 13

4.4 Instrumentation 13

4.5 Positioning 15

4.6 Signal Processing 16

4.7 CT Analysis 16

5. Results 17

5.1 Sustained Injuries 18

5.2 Spinal Acceleration 18

5.3 Spinal Kinematics 21

5.4 CT Bone Density 22

6. Discussion 24

7. Conclusions 26

Appendix A: Measured System and Spinal Responses 28

Bibliography 36

Curriculum Vitae 42

List of Figures

FIG. 1. (LEFT) LATERAL VIEW OF SPINAL REGIONS AND THEIR ASSOCIATED NATURAL CURVATURE IN THE STANDING POSITION. (HTTP://WWW.SPINEUNIVERSE.COM/ANATOMY/SPINAL-CURVES) STRAIGHTENING OF LUMBAR SPINE CURVATURE BETWEEN STANDING (MIDDLE) AND SEATED (RIGHT) POSITION (STUMPF 1995).....4

FIG. 2. SAGITTAL CROSS-SECTION OF LUMBAR VERTEBRAE SHOWING CORTICAL SHELL AND CANCELLOUS BONE (HTTP://DESIGN.AE.UTEXAS.EDU/SPINE/FINAL.HTML) 5

FIG. 3. INTERVERTEBRAL DISC OF LUMBAR VERTEBRAE SHOWING ANNULUS AND NUCLEUS (HTTP://WWW.MAYFIELDCLINIC.COM/PE-ANATSPINE.HTM) 5

FIG. 4. AXIAL AND POSTERIOR VIEW OF THORACIC SPINE SHOWING STRUCTURE AND INTERACTION OF POSTERIOR ELEMENTS (HTTP://WWW.MAYFIELDCLINIC.COM/PE-ANATSPINE.HTM).....6

FIG. 5. LUMBAR VERTEBRAE DEPICTION OF SPINAL LIGAMENTS (HTTP://WWW.MAYFIELDCLINIC.COM/PE-ANATSPINE.HTM) 7

FIG. 6. (LEFT) CAD MODEL OF VALTS, (RIGHT) VALTS SETUP WITH PMHS SPECIMEN IN SEATED POSITION PRE-TEST 11

FIG. 7. (TOP LEFT) FRONTAL X-RAY SHOWING METALLIC PINS USED TO DETERMINE LOCATION AND TRAJECTORY OF PEDICLE SCREWS, (BOTTOM LEFT) LATERAL X-RAY SHOWING INSTALLED T12 SPINAL 6DX BLOCK, (MIDDLE) SEATED X-RAY OF SPINAL ALIGNMENT PRIOR TO TEST EXECUTION. (RIGHT) PICTORIAL REPRESENTATION OF SAEJ211 COORDINATE SYSTEM USED FOR INTERPRETATION OF BODY RESPONSES. (SAE 2003).....14

FIG. 8. (LEFT) CT RECONSTRUCTION OF TESTED PELVIS REGISTERED TO THE PRE-TEST POSITION USING CMM DATA. (RIGHT) PELVIS POSITION BASED ON SEATED SOLIDER STUDY SHOWING TARGET PELVIS POSITION OF 40° BONE ANGLE.....16

FIG. 9. CT SLICE DEPICTION OF THE ELLIPTICAL REGIONS UTILIZED TO CHARACTERIZE THE BONE DENSITY FOR EACH VERTEBRAL BODY. 17

FIG. 10. T12 SAGITTAL (X AND Z) ACCELERATION RESPONSES FROM SPINAL 6DX MOUNTS AT MILD, MODERATE, AND SEVERE CONDITIONS. THE SEVERE CASES SHOW LATE PHASE NOISE WHICH WAS

associated with spinal injury. The mild condition (dashed line) is an average response of the four tests. 19
Fig. 11. Average peak resultant acceleration in the sagittal plane across the PMHS spine.....19
Fig. 12. Characteristic full spine axial (Z) acceleration response to Condition A (mild severity) showing phasing of onset as well as peak magnitude reduction.....20
Fig. 13. Observation of the effect of bridging osteophytes: (left) Spine without osteophytes shows a 1.8 ms phasing between onset at T5 relative to T12, (right) Spine with bridging osteophytes from T12 to T6 shows a 0.4 ms (80% reduction) phasing between onset at T5 relative to T12 21
Fig. 14. Characteristic spinal angular rate response at Condition A (low severity) 22
Fig. 15. Relative spinal segment rotation between upper and lower vertebral bodies. Condition C (severe case) sustained a vertebral body fracture at T12 prior to peak rotation.....22

Figure A.1 System input acceleration and velocity for Condition A: Test 1 28
Figure A.2 System input acceleration and velocity for Condition A: Test 2 28
Figure A.3 System input acceleration and velocity for Condition A: Test 3 29
Figure A.4 System input acceleration and velocity for Condition A: Test 4 29
Figure A.5 System input acceleration and velocity for Condition B: Test 1....29
Figure A.6 System input acceleration and velocity for Condition B: Test 2....30
Figure A.7 System input acceleration and velocity for Condition C: Test 1....30
Figure A.8 Spinal angular rotation and velocity for Condition A: Test 1....30
Figure A.9 Spinal angular rotation and velocity for Condition A: Test 2....31
Figure A.10 Spinal angular rotation and velocity for Condition A: Test 3....31
Figure A.11 Spinal angular rotation and velocity for Condition A: Test 4....31
Figure A.12 Spinal angular rotation and velocity for Condition B: Test 1 32
Figure A.13 Spinal angular rotation and velocity for Condition B: Test 2....32
Figure A.14 Spinal angular rotation and velocity for Condition C: Test 1 32

FIGURE A.15 SPINAL SAGITTAL ACCELERATION RESPONSES (X AND Z) FOR CONDITION A: TEST 1 33

FIGURE A.16 SPINAL SAGITTAL ACCELERATION RESPONSES (X AND Z) FOR CONDITION A: TEST 2 33

FIGURE A.17 SPINAL SAGITTAL ACCELERATION RESPONSES (X AND Z) FOR CONDITION A: TEST 3 33

FIGURE A.18 SPINAL SAGITTAL ACCELERATION RESPONSES (X AND Z) FOR CONDITION A: TEST 4 34

FIGURE A.19 SPINAL SAGITTAL ACCELERATION RESPONSES (X AND Z) FOR CONDITION B: TEST 1.....34

FIGURE A.20 SPINAL SAGITTAL ACCELERATION RESPONSES (X AND Z) FOR CONDITION B: TEST 2.....34

FIGURE A.21 SPINAL SAGITTAL ACCELERATION RESPONSES (X AND Z) FOR CONDITION C: TEST 1.....35

List of Tables

TABLE 2. ACHIEVED VALTS SEAT AND FLOOR INPUT CONDITIONS.....12

TABLE 1. EXPERIMENTAL SPECIMEN POSITIONING 15

TABLE 3. SUMMARY OF MEAN HU VALUES FOR EACH VERTEBRAL BODY ANALYZED WITHIN EACH TESTED SPECIMEN. THE GRADIENT FROM LIGHT TO DARK INDICATES DECREASING HU VALUES RELATIVE TO THE SET. BOXED VALUES ARE VERTEBRAL BODIES THAT SUSTAINED INJURIES DURING TESTING. 23

1. Introduction

Military vehicles have evolved in recent history to become more resistant to improvised explosive devices (IED), but the massive amount of energy imparted during under-body blast (UBB) events still causes debilitating injuries to vehicle's occupants. UBB events are characterized by short duration, high amplitude accelerative loading delivered through the vehicle structure both directly to the occupant and through the seat system (Arepally 2008). This type of loading induces a range of injuries to the occupants from head and neck injuries (Gondusky 2005), to upper and lower extremities injuries (Owens 2007; Ramasamy 2008), to spinal injuries primarily in thoracolumbar junction and lumbar region (Blair 2011; Ragel 2009; Stemper 2012; Possley 2011). These spinal injuries are of particular concern due to the risk of spinal cord damage and long term effects on quality of life. Current anthropomorphic test dummies (ATD) are limited in their ability to predict the human body response to these events (Bailey 2013).

Anatomically, the thoracolumbar spine describes the region bounded superiorly by T7 and inferiorly by L5 (Yoganandan 2013). This region is characterized by a transition in curvature from the lordosis of the lumbar spine to kyphosis of the thoracic spine, both of which are accentuated in the standing position. In the seated position, the lumbar spine straightens to become more vertical; this straightening typically results in the thoracolumbar spine being the spinal region most aligned with vertical loading direction. The thoracolumbar spine is also the only skeletal support connecting the pelvis to the mass of the torso. Therefore, during a vertical acceleration, such as a UBB event, the thoracolumbar spine becomes the primary load path for supporting the inertial mass of the torso. Due to the variable positioning and challenges with representation of the torso mass, testing the fully intact spine has a high degree of complexity.

High rate injury biomechanics has widely focused on decelerations in the horizontal direction, motivated primarily by civilian automotive impacts. These impacts and the resulting

human response has been studied in the frontal (Petitjean 2002), side (Pintar 2007), and rear impact conditions (Michaelson 2008). The horizontal impact studies characterized the human response to frontal, side, and rear loading scenarios so that better safety systems could be devised and ultimately, lives could be saved. Further, horizontal impact studies have been critical in the development of ATDs that are able to accurately and consistently represent the human response to loading in the horizontal plane. These ATDs have allowed for researchers to explore the effects of various rates and directions of horizontal loading and the resulting predicted injury response.

However, there remains a significant lack of understanding regarding human body response and injury tolerance for vertical inertial loading. Literature exists on vertical events, such as aircraft ejections, which occur over a longer duration (>100 ms, Salazar 2009) and with a lower magnitude of acceleration as compared to UBB events (Stemper 2012). The most commonly used ATDs for these vertical impact studies were the Hybrid dummies (Humanetics Innovative Solutions, Plymouth, MI) which were originally designed for replicating the human body response to horizontal impacts. Salzar et al. compared the results of simulated pilot ejections with the Hybrid III ATD and post-mortem human subjects (PMHS), showing differing kinematic responses between the PMHS and ATD. Polanco investigated the response of Hybrid II and Hybrid III ATDs in drop tower tests at high acceleration, short durations and low acceleration, long duration and compared his results to commercially available ATD computational models. The results of Polanco's work showed major differences between the Hybrid II and III ATDs as well as between the ATDs and computational models. Some of the difficulties of testing with the current ATDs is that their construction incorporates non-compliant elements such as a solid metallic thoracic spine and rib cage, as well as a lumbar spine component with a kyphotic curvature, opposite of the normal human anatomy. While the undesirable effect of the non-compliant elements and unhuman like, or non-biofidelic, curvature has been mitigated to some degree by the replacement of certain components (Gowdy 1999; Polanco 2011), the overall

PMHS response characteristics have not been compared to ATDs in the vertical direction. Further advances in injury mitigation require both an expanded knowledge of the human response to vertical loading and the development of tools to predict injury risk due to vertical loading.

The inadequacy of ATDs to accurately represent the human body response to vertical loading is a gap which can be resolved with further study. The aim of this effort was to characterize the non-injurious response of the PMHS spine under three different loading conditions relevant to the UBB environment, with a secondary aim of determining response and specimen characteristics that could be predictive of spinal injury. The hypothesis being that the thoracolumbar spine is most susceptible to fracture due to it seeing the maximum acceleration in the spine and its optimal alignment to the vertical loading condition. These factors, combined with the lumbar spine being the only structure supporting the mass of the torso, should cause large internal loads leading to a high risk of fracture.

2. Spine Anatomy

The human spinal column consists of 33 vertebral segments connected by intervertebral discs, facet joints, and a multitude of ligaments. There typically are seven cervical vertebrae, twelve thoracic, five lumbar, five vertebrae fused to form the sacrum, and another four vertebrae fused forming the coccyx. The cervical spine extends from the inferior base of the skull to the top of the ribcage. The thoracic spine spans the length of the ribcage and provides anchorage for the posterior aspect of the ribs. The lumbar spine is located in the abdominal region and ends at the sacrum. The sacrum and coccyx combine to create what is widely known as the “tailbone”. Both the cervical and lumbar regions have an anteriorly convex shape, or lordosis. The thoracic region has an anteriorly concave shape, also known as kyphosis. For the purposes of the current study, focus will be placed on the cervical, thoracic, and lumbar regions. (Figure 1)

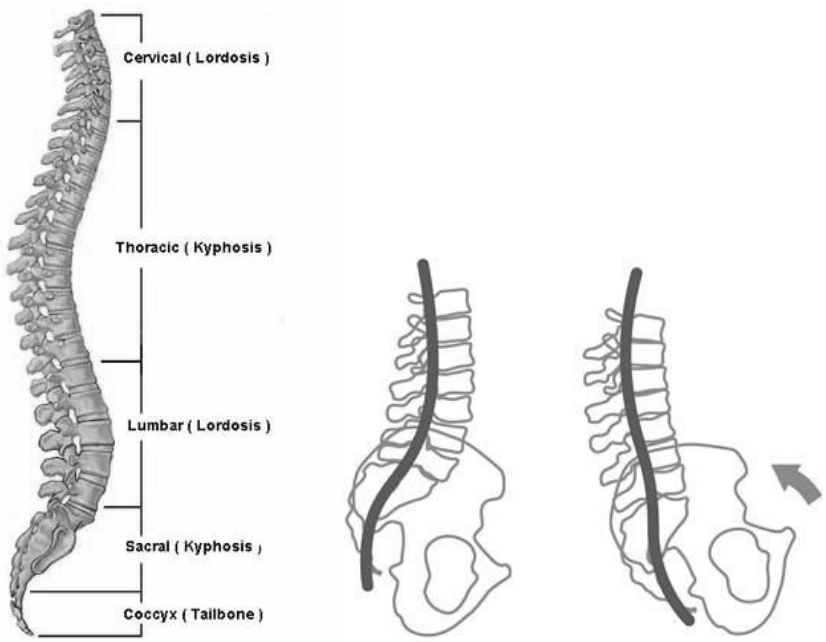

Fig. 1. (left) Lateral view of spinal regions and their associated natural curvature in the standing position. (http://www.spineuniverse.com/anatomy/spinal-curves) Straightening of lumbar spine curvature between standing (middle) and seated (right) position (Stumpf 1995).

While each region has its own distinct features, all vertebrae in the regions of interest share common structural features. Vertebral bodies, the cylindrical, anterior portion of the vertebrae consists of a superior and inferior endplate, a cortical shell, and a "spongy" cancellous bone core. (Figure 2) The endplates create the superior and inferior surfaces through which the vertebral body connects to the intervertebral discs. Vertebral endplates are formed of a thin layer of hyaline cartilage fused to the vertebral body. The cortical shell, which encapsulates the vertebral body, is thin, 0.64 ± 0.41 mm (Edwards 2001), with a Young's modulus nearly double that of the cancellous, or trabecular, bone that is organized in a lattice-like structure inside the cortical shell to resist axial force while minimizing weight. The density of the cancellous bone is often quantified by CT measurements or dual-energy X-ray absorptiometry (DEXA) and is correlated to compressive strength as the square of density. The vertebral body is the primary load path during vertical loading.

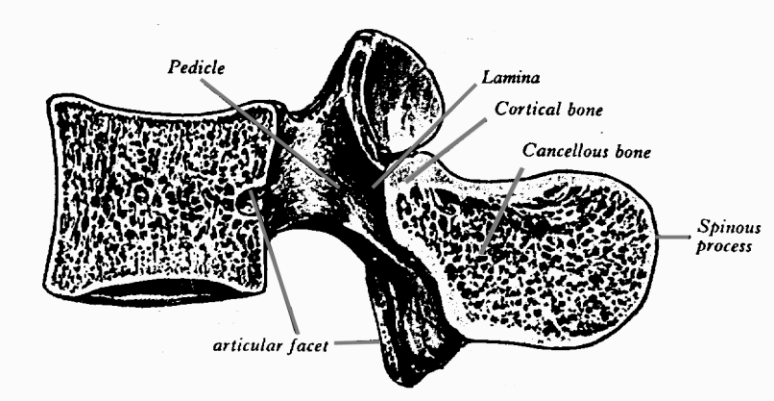

Fig. 2. Sagittal cross-section of lumbar vertebrae showing cortical shell and cancellous bone (http://design.ae.utexas.edu/spine/final.html)

Intervertebral discs form the primary articulation surface between neighboring vertebral bodies. (Figure 3) They are fibro-cartilaginous joints constructed of two distinct regions. The annulus fibrosus is the region of concentric rings of collagen fibers that are arranged along the periphery of the intervertebral disc. The center of the disc is referred to as the nucleus pulposus and has a viscoelastic behavior which assists in the absorption and dampening of shock. The purpose of the disc as a whole is to resist axial compression, tension, rotation, and lateral and antero-posterior shear.

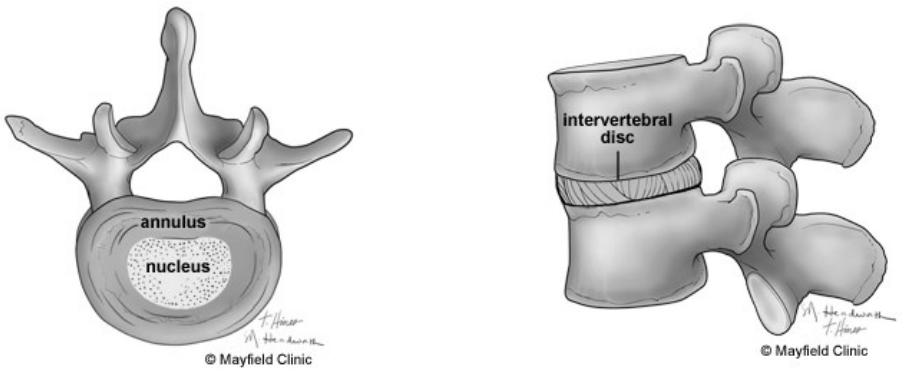

Fig. 3. Intervertebral disc of lumbar vertebrae showing annulus and nucleus (http://www.mayfieldclinic.com/PE-AnatSpine.htm)

The posterior elements of vertebrae are the bony elements that emanate from the superior, posterior aspect of the vertebral body and encapsulate the spinal column. (Figure 4) The pedicles attach directly to the vertebral body anteriorly and terminate at the lamina which forms the posterior border for the spinal canal. The spinous process is located medially and extends posteriorly from the lamina. The spinous process has a distinctly different shape in the lumbar, thoracic, and cervical spinal regions. The transverse processes extend laterally from the pedicles on both the left and right. In the thoracic spine, the transverse processes are the posterior insertion points for the ribs. Finally, the superior and inferior articular processes are located near the intersection of the lamina and the pedicles and interact to create the facet joints between vertebrae.

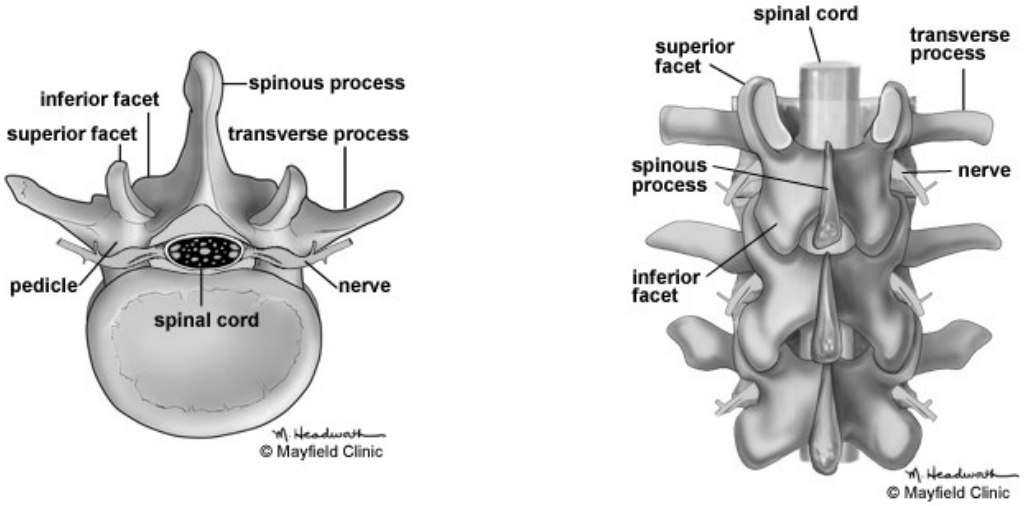

Fig. 4. Axial and posterior view of thoracic spine showing structure and interaction of posterior elements (http://www.mayfieldclinic.com/PE-AnatSpine.htm)

The facet joints are the posterior-lateral articulation surfaces of vertebrae joints. (Figure 4) The surfaces are covered with a layer of hyaline cartilage and the joint is encapsulated in capsular cartilage. The capsule is filled with synovial fluid which allows for a smooth gliding motion while the collagen rich cartilage prevents joint distraction. The facet joints provide antero-

posterior stability to the spine as well as some vertical and rotational stability. The facets provide a secondary load path during vertical loading of the spine.

A major component of spinal stability that is not a focus of this study is the spinal ligaments. (Figure 5) The major spinal ligaments are the anterior longitudinal ligament (ALL) that runs along the anterior aspect of the spine from the skull base to the sacrum connecting to the anterior aspects of the vertebral bodies. The posterior longitudinal ligament (PLL) runs along the posterior aspects of the vertebral bodies through the spinal canal. The interspinous ligaments connect neighboring spinous processes along their length while the supraspinous ligaments connect the most posterior aspect of the spinous processes. The inter- and supraspinous ligaments provide support to flexion of the spine.

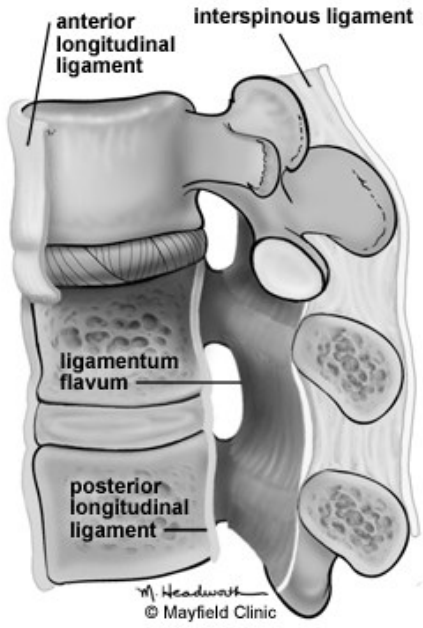

Fig. 5. Lumbar vertebrae depiction of spinal ligaments (http://www.mayfieldclinic.com/PE-AnatSpine.htm)

3. Literature Review

3.1 Whole Body Testing

The field of impact biomechanics began in earnest in 1939 when Gurdjian and Lissner founded the Bioengineering Center at Wayne State University for the purpose of conducting experimental testing on post-mortem human subjects (PMHS) to better understand head injury thresholds. In the subsequent 76 years, numerous laboratories and test facilities across the world have undertaken the study of impact biomechanics to better understand the response of the human body to a wide variety of loading cases. Occupant protection research test subjects have consisted of human volunteers (Stapp 1951, 1962), PMHS (Bailey 2013, Michaelson 2008, Pintar 2007), animals (Kazarian 1970), or anthropomorphic test dummies (ATDs) such as the Hybrid III (Bailey 2013, Petitjean 2002, Polanco 2011), Hybrid II (Polanco 2011), Thor (Petitjean 2002, Pintar 2007), or modified versions of the aforementioned ATDs (Gowdy 1999).

While each different type of test subject has its advantages and unique challenges, ATDs offer the simplest option from an engineering perspective. They are designed to be durable and repeatable in multiple loading conditions and equipped with sensors, such as load cells and in-line accelerometers, which would be difficult to incorporate into other test subjects without disrupting critical structures. Repeatability is achieved by removing degrees of freedom from ATDs in directions that are non-critical to the loading they are designed for, such as horizontal loading for the Hybrid dummies. This is especially true for the spine, a region of complex interactions that are not of primary focus in horizontal loading due to lack of real-world injury. Using ATDs designed for horizontal loading conditions to better understand the response to a vertical loading condition can create sensor responses that would falsely predict human injury (Gowdy 1999, Bailey 2013).

In the vertical loading condition, PMHS have been used frequently because they offer the best combination of biofidelity, versatility of instrumentation, and clarity in the interpretation of response. Examples of vertical loading environments that have been examined with prior PMHS

testing are ejection seat loading, helicopter crashworthiness, land mine blasts, and high speed hydroplaning watercraft. The most direct correlate to UBB loading of this set is ejection seat loading, which was originally studied because of the high incidence of vertebral fracture during emergency egress from aircrafts (King 1973, Glaister 1965). Early PMHS studies exposed subjects to vertical accelerations, incident at the pelvis, resulting in flexion of the head and sustained anterior compression fractures of the thoracolumbar region (Vulcan 1970, Ewing 1972). These studies highlighted the importance on bending to injury creation and that manipulation of spinal posture can increase the injury threshold of PMHS subjects.

3.2 Component Level Testing & Injury Mechanisms

To achieve greater postural control and allow for the measurement of boundary conditions that would otherwise be impossible with whole body PMHS, component level testing has been done to identify response characteristics at the vertebrae component and motion segment (2 or more vertebrae) level. The following section explores the current state of the science for component level testing identifying injury mechanisms and thresholds.

For the purpose of identifying mechanical properties of different components of the vertebrae, commonly for finite element modeling, individual vertebral body testing is done at a variety of loading rates. Studies have been done looking at the overall vertebrae to isolate the effect of loading rate on fracture mechanics (Dooley 2012, Stemper 2015, Belkoff 2001). For high fidelity FE models, it is also necessary to determine the pre-failure properties of all vertebral components such as endplates, cortical shell, trabecular core, as well as the facet joints (MacLean 2007, Eswaran 2006, van der Veen 2008, Oxland 2003). FE studies have been done, using the experimentally derived properties, to investigate other parameters such as age, disc degradation, and other factors that are hard to control based on specimen acquisition (Christiansen 2010, Silva 1997).

To investigate injury types other than compression fractures, as well as highlight the bending behavior of the spine, motion segments of three vertebral levels or greater have been studied both experimentally and computationally. Denis (1983) provides a comprehensive review of the four main injury types, compression fracture, burst fracture, seat-belt-type (also known as chance fractures), and fracture dislocation, and the modes in which they occur in motion segments. More recently, studies have been done to recreate specific injuries seen in environments, such as UBB events, in order to assist in their prevention (Langrana 2001, Stemper 2014, Zhang 2011). Other studies have looked at the behavior of the spine in bending to further understand the interaction of its complex structure (Patwardhan 1998, Zhang 2013, Lu 2013).

3.3 Bone Quality Assessment

Bone quality measurements, such as quantitative computed tomography (qCT) and dual-energy x-ray absorptiometry (DEXA), have been used as a metric for analysis in the aforementioned studies. It can be used as a specimen selection criterion to ensure that a PMHS falls within a representative range based on medical data and the population being investigated. Schreiber et al correlated qCT measurements in Hounsfield units to DEXA scores, a more clinically relevant assessment of bone quality. Other studies, such as Kopperdahl et al, have associated qCT measurements to material properties such as yield stress and Young's modulus.

4. Materials and Methods

This protocol was reviewed and approved by the U.S. Army Medical Research and Material Command Office of Research Protections based on the U.S. Army Policy for Use of Human Cadavers for Research, Development, Test and Evaluation, Education, or Training on February 6th, 2013.

4.1 Test Device

The Vertically Accelerated Load Transfer System (VALTS) has been developed to create floor and seat pulses representative of the UBB vehicle loading environment. Standing at a total height of 10.5 meters, the VALTS has the capacity to be able to simultaneously provide vertical loading to two specimen or test devices. The system features controlled vertical accelerative impulse to the test specimen body (i.e., simulating global accelerative loading), and controlled decelerative impulse to the test specimen body (i.e., simulating slam-down impact of the vehicle). The current study focuses only on the accelerative portion of the UBB event. Additionally, due to the unique nature of the UBB loading environment, the VALTS includes separately controllable floor and global body load platforms which allow for the simulation of different loading rates and magnitudes of the vehicle floor and superstructure. Achieved velocity ranges for the VALTS range from 2 to 10 m/s with durations of 5 to 40 ms for the carriage and 7 to 16 m/s with durations of 2 to 10 ms for the floor.

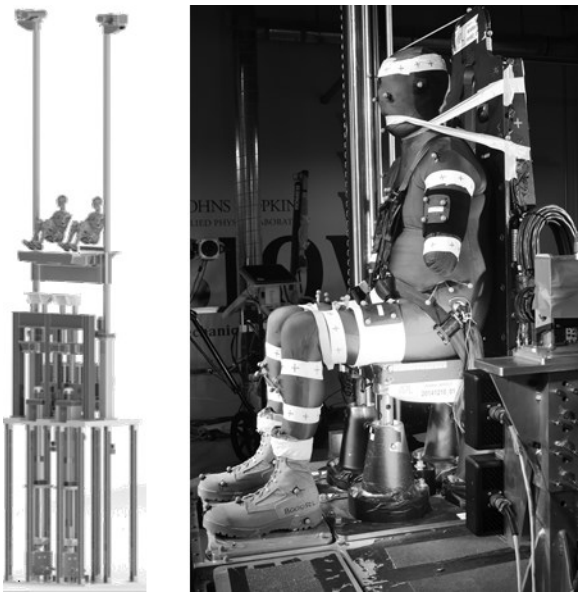

Fig. 6. (left) CAD model of VALTs, (right) VALTs setup with PMHS specimen in seated position pre-test

An aluminum seat designed with dimensions relevant to fielded seat systems and incorporating a five point belt was used for this study. (Figure 6) Load profiles to the floor and seat were determined by comparisons to UBB response data with a focus on the sub-injurious levels of exposure.

4.2 Experimental Input Conditions

Three loading conditions were used, representing varying severity levels. Simultaneous floor and seat motion was used for all conditions.

- Condition A: Mild exposure, 4 m/s peak velocity with 5 ms time to peak (TTP) on both the floor and seat.
- Condition B: Moderate exposure, 4 m/s velocity with 10 ms TTP on the seat, 6 m/s velocity with 5 ms TTP on the floor.
- Condition C: Severe exposure, 6 m/s velocity with 10 ms TTP on the seat, 8 m/s velocity with 5 ms TTP on the floor.

Each PMHS was exposed to a single impact at one of the three different loading conditions, summarized in Table 2. Timing of the loading to the floor and seat achieved a differential of 0.5 ± 0.9 ms, where positive timing indicates the floor loading preceding the seat loading.

Table 1. Achieved VALTs seat and floor input conditions

	Condition		
	A (n = 4)	**B** (n = 2)	**C** (n = 1)
Peak Seat Accel. (g)	242.9 ± 47.2	136.2 ± 31.2	157.9
Peak Seat Vel. (m/s)	3.8 ± 0.5	4.2 ± 0.2	5.8
Time-To-Peak (ms)	5.6 ± 0.3	9.1 ± 0.2	9.6
Peak Floor Accel. (g)	143.8 ± 20.2	255.1 ± 9.0	362.8
Peak Floor Vel. (m/s)	3.8 ± 0.5	6.1 ± 0.0	8.2
Time-To-Peak (ms)	4.2 ± 0.1	4.1 ± 0.2	4.6

4.3 Tested Surrogates

Specimen variability was minimized through restrictions on anthropometry and bone quality. The targeted specimen was between 18 and 80 years of age with anthropometry within one standard deviation of the 50th percentile military male and a DEXA Lumbar t-score between -1 and 2.5. The average specimen was 72 ± 3.3 years of age, weighed 82.5 ± 10.6 kg, and had a total stature of 177.6 ± 6.4 cm. Average specimen BMI was 26.2 ± 3.1 and Lumbar t-Score was 1.22 ± 0.09. Specimens with prior traumatic injuries to the spine, skull, or long bones, as well as specimen with spinal deformities such as bridging osteophytes and degenerative discs, were excluded from the study based on review from a radiologist and biomechanics experts.

4.4 Instrumentation

In order to characterize the timing, magnitude and transmission of the loading pulse from the system, the PMHS was instrumented with a suite of sensors to record both the local mechanical response of individual segments as well as the overall kinematic response. These sensors included three axis acceleromoters and angular veclocity sensors (6DX PRO 2k-18k, DTS, Seal Beach, CA). These sensors were mounted to bony anatomy of the specimen through custom designed mounts that were matched to the specimen's specific spinal geometry. To install these mounts along the spine, the targeted vertebral levels were located through palpation and verified through use of a lateral X-ray. With the skin retracted, bilateral vertical incisions were made along the lateral edges of the supraspinous ligament allowing for access to the posterior surface of the lamina. The facets were then located using metallic pins in conjunction with a P-A X-ray to determine insertion trajectory. The mounting block was then sized to minimize the offset from the lamina without contacting the spinous processes. (Figure 7)

Attached to the posterior surface of the spine mounts by threaded rod were four marker kinematic tracking blocks which were optically tracked by a 16-camera Vicon system sampling at 1000 frames per second (fps). In addition, kinematic response data was also captured by four high

speed cameras sampling at 7500 fps for the frontal and lateral views (Phantom v711, Vision Research, Wayne, NJ)., 5000 fps for the posterior view (Phantom v10, Vision Research, Wayne, NJ)., and an onboard, shock resistant camera sampling at 1200 fps (Phantom Miro3, Vision Research, Wayne, NJ).

Additionally, accelerometers were used to measure both the system input (Endevco 7270A-6k, Meggitt Sensing Systems, Irvine, CA) to the PMHS as well as the response at areas where specimen geometry constrained the amount of available space for sensor installation (Endevco 7264C-2k, Meggitt Sensing Systems, Irvine, CA). Finally, in addition to these sensor types, strain gages (C2A-06-062LW-350, Vishay Precision Group, Wendell, NC) and acoustic sensors (PICO 200-750 kHz, Physical Acoustics, Princeton Junction, NJ) were used to determine the presence and timing of any fractures that occurred during testing. All sensor data was recorded at 1 MHz and body responses were interpreted using the SAE J211 coordinate system (SAE 2003, Figure 7).

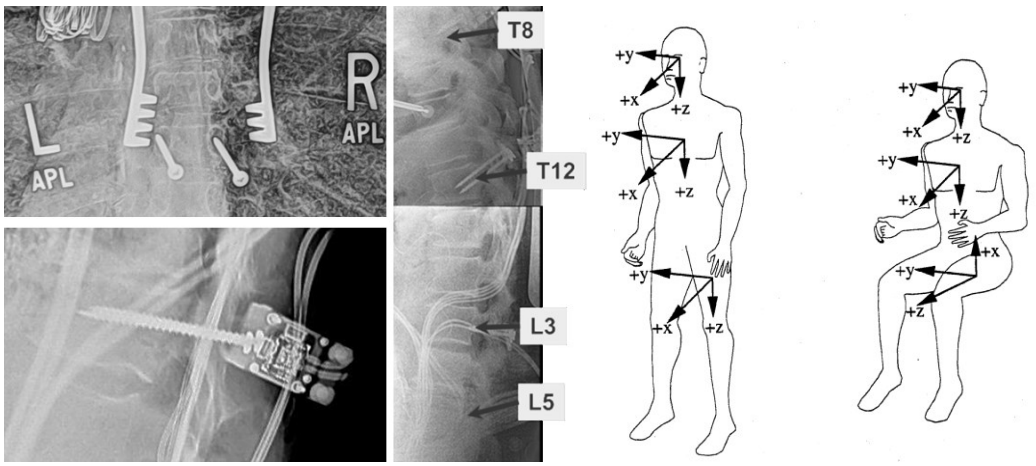

Fig. 7. (top left) Frontal X-ray showing metallic pins used to determine location and trajectory of pedicle screws, (bottom left) Lateral X-ray showing installed T12 spinal 6DX block, (middle) Seated X-ray of spinal alignment prior to test execution. (right) Pictorial representation of SAEJ211 coordinate system used for interpretation of body responses. (SAE 2003)

4.5 Positioning

Each specimen was positioned in an upright seated condition. Targeted anatomical landmarks developed from a seated soldier study were used to guide the positioning of each specimen (Reed 2013). Thirteen metrics were used to define correct specimen orientation prior to testing. (Table 1) A 90° angle between the floor and tibia, as defined as the vector between the lateral tibial condyle and lateral malleolus, as well as tibia and femur, as defined by the vector between the greater trochanter and lateral femoral epicondyle, was achieved for positioning of the legs. Vertical and fore-aft differences between the left and right anterior superior iliac spine (ASIS) and left and right acromion process were used to align the shoulders and hips. A 40° bony angle of the pelvis with respect to the global vertical axis, as defined by the plane created by the left and right ASIS and the pubic symphysis, was achieved to align with the seated soldier study. (Figure 8) The distance from the midpoint of the ASIS' to the cervicale, the most posterior point of the C7 spinous process, was controlled for upright posture. Alignment of the head was achieved by positioning the tragion, a point in the notch of the ear anterior of the auditory canal, anterior of the cervicale and inferior of the infraorbitale, the most inferior point of the ocular cavity near the intersection of the maxilla and the zygomatic arches.

Table 2. Experimental specimen positioning

Positioning Req't	Targeted Position	Achieved Position
Pelvis Angle (°)	40 ± 5	42.6 ± 3.2
Foot Angle (°)	90 ± 2	90 ± 1
Knee Angle (°)	90 ± 2	90 ± 1
ASIS Fore-Aft Difference (mm)	0 ± 10	0.9 ± 3.7
ASIS Vertical Difference (mm)	0 ± 10	2.2 ± 3.5
ASIS aft to Cervicale (mm)	90 ± 10	87.0 ± 6.3
Acromion Fore-Aft Difference (mm)	0 ± 20	0.6 ± 8.7
Acromion Vertical Difference (mm)	0 ± 20	9.8 ± 11.2
Tragion aft to Cervicale (mm)	85 ± 10	85.2 ± 5.7
Infraorbitale superior of Tragion (mm)	10 ± 5	8.9 ± 3.3
Boot Heels Separation (mm)	295 ± 10	294.6 ± 1.4
Boot Toe Separation (mm)	295 ± 10	294.6 ± 1.4
Mid-Patella Separation (mm)	295 ± 10	294.6 ± 1.4

Positioning was confirmed through lateral X-rays as well as use of a coordinate measurement machine (CMM). The CMM was used to digitize anatomical landmarks and rigid sensor mounts immediately prior to execution of the test and allowed for comparison of position repeatability across tests

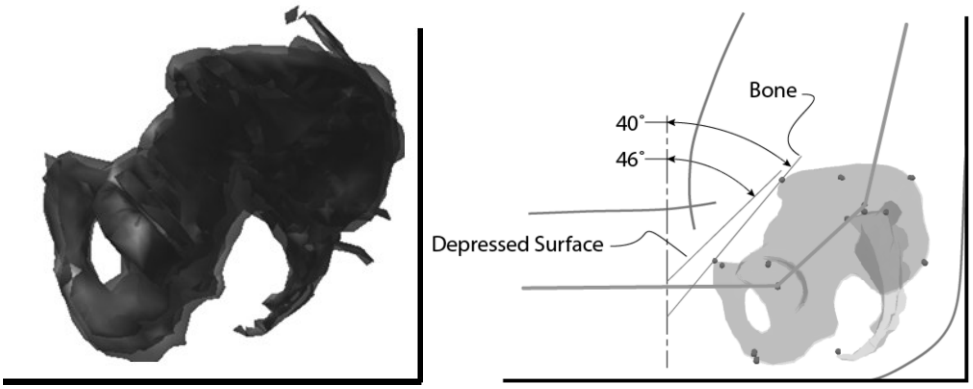

Fig. 8. (left) CT Reconstruction of tested pelvis registered to the pre-test position using CMM data. (right) Pelvis position based on seated solider study showing target pelvis position of 40° bone angle

4.6 Signal Processing

Based on spectral analysis of the recorded signals, both accelerometers and angular velocities were filtered using 4-pole Butterworth low pass filters at 3000 kHz and 1650 Hz respectively. These filter specifications were selected to maintain the relevant response while eliminating potential noise in the signal response. Acoustic signals were filtered with a 4-pole Butterworth high pass filter at 20 (Allsop, 1991, Funk 2002, Cormier 2008, Van Toen 2012).

4.7 CT Analysis

Whole body CT scans with a slice thickness of 0.625 mm were taken prior to testing. Individual vertebrae in the pre-test CT were analyzed to determine average Hounsfield unit (HU) intensities at three levels using an analysis technique adopted from Schrieber et al. The three

elliptical regions of interests (ROI) per vertebral body were manually delineated on axial slices of the CT scan: one immediately inferior to the superior endplate, one in the middle of the vertebral body, and one immediately superior to the inferior endplate (Figure 9). Each ROI was drawn as large as possible within the vertebral body while avoiding cortical bone, and the areal mean intensities were calculated for each ROI. All three mean intensities were then averaged to compute a final mean HU intensity for each vertebral body. A one-tailed t-test was conducted between the mean HU intensities of the fractured vertebral bodies and those of the uninjured bodies to test the hypothesis that the mean of the population of all fractured bodies is less than that of the unfractured bodies. We conducted the analysis using the open source image software, FIJI, which is a distribution of the image analysis software known as ImageJ (Schindelin 2012, Schneider 2012).

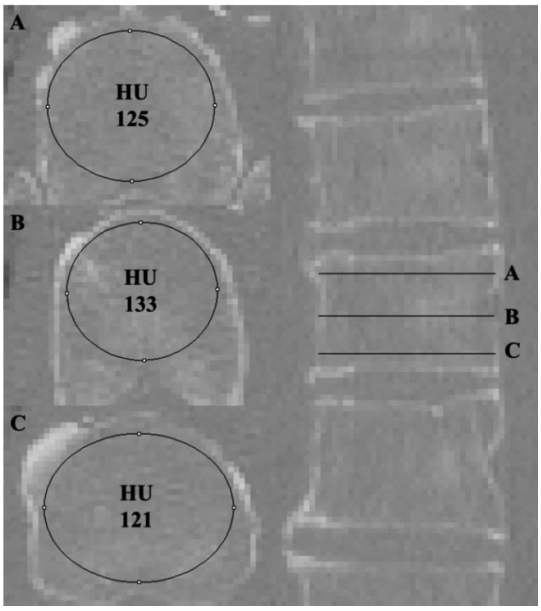

Fig. 9. CT slice depiction of the elliptical regions utilized to characterize the bone density for each vertebral body.

5. Results

5.1 Sustained Injuries

Injuries were observed in 4 of the 7 tests that were executed under Conditions A-C. One of the four specimens at Condition A sustained a single transverse process fracture at each L4 and L5 which were characterized as mild injuries.

Of the two specimen exposed to Condition B, one sustained a bilateral transverse process fracture of L4, a single transverse process fracture at L2, and a non-displaced, no loss of vertebral body height based on CT scan, compression fracture at L4. The other Condition B specimen sustained a non-displaced compression fracture of T6 and a fracture of the 6th rib on the right side. Both injury cases were characterized as moderate injuries because of the minimal loss of vertebral body height in the compression fractures.

The single specimen at Condition C sustained comminuted fracture of the right iliac wing, fracture of the left body of the sacrum, and a displaced compression fracture of T12. These were categorized as severe injuries.

5.2 Spinal Acceleration

Sagittal accelerations are shown in Figure 10 for each condition. Condition A and B, the low and moderate cases respectively, show a similar initial rise and peak but Condition A, due to having a shorter duration input shows an earlier unloading response as indicated by the 47% reduction in magnitude in the Z direction between 4.5 and 6 milliseconds. Condition B and C achieved longer sustained peak accelerations. Condition C, the severe case, displays unstable behavior after 7 ms, the reason for this was structural failure of the T12 vertebral body.

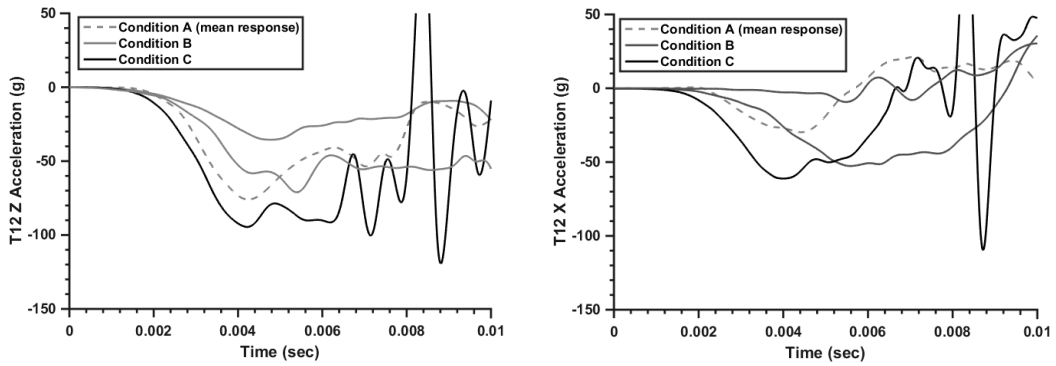

Fig. 10. T12 sagittal (X and Z) acceleration responses from spinal 6DX mounts at mild, moderate, and severe conditions. The severe cases show late phase noise which was associated with spinal injury. The mild condition (dashed line) is an average response of the four tests.

Peak resultant accelerations in the sagittal plane, distributions where applicable, are shown in Figure 11. At each condition, the maxima resided in the thoracolumbar region. For Condition A, T12 showed the highest mean response at 100.4 ± 20.6 g. Condition B and C showed a maxima occurring at L3 at 81.2 ± 13.1 g and 139.9 g respectively. The primary component of the resultant at each level, across all conditions, was in the axial (Z) direction with a mean contribution of 88.8% to the peak resultant.

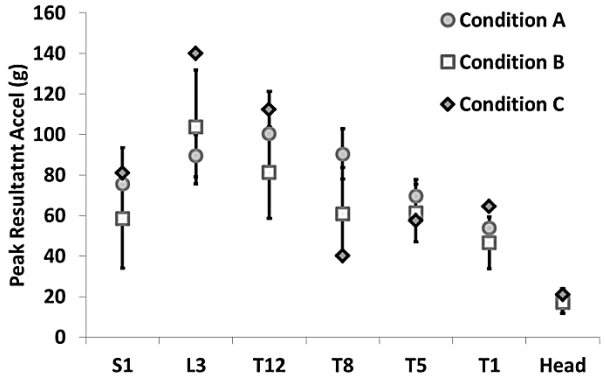

Fig. 11. Average peak resultant acceleration in the sagittal plane across the PMHS spine

An example of a full spine response can be seen in Figure 12. Of note is the phasing of the acceleration transmission up the spine. From the onset of acceleration at the sacrum (1.5 ms) to arrival of the pulse at the T1 spinal level (3.5 ms), the total duration is approximately 2 ms. When bridging osteophytes were present in the spine, a single case, the delay between onset at neighboring segments was shortened by over 80% and seemed to be experienced nearly simultaneously. (Figure 13)

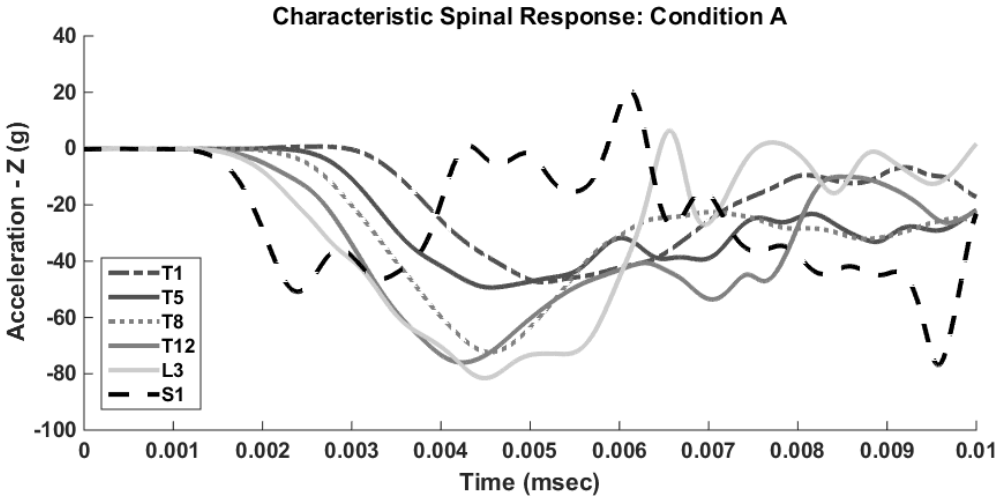

Fig. 12. Characteristic full spine axial (Z) acceleration response to Condition A (mild severity) showing phasing of onset as well as peak magnitude reduction.

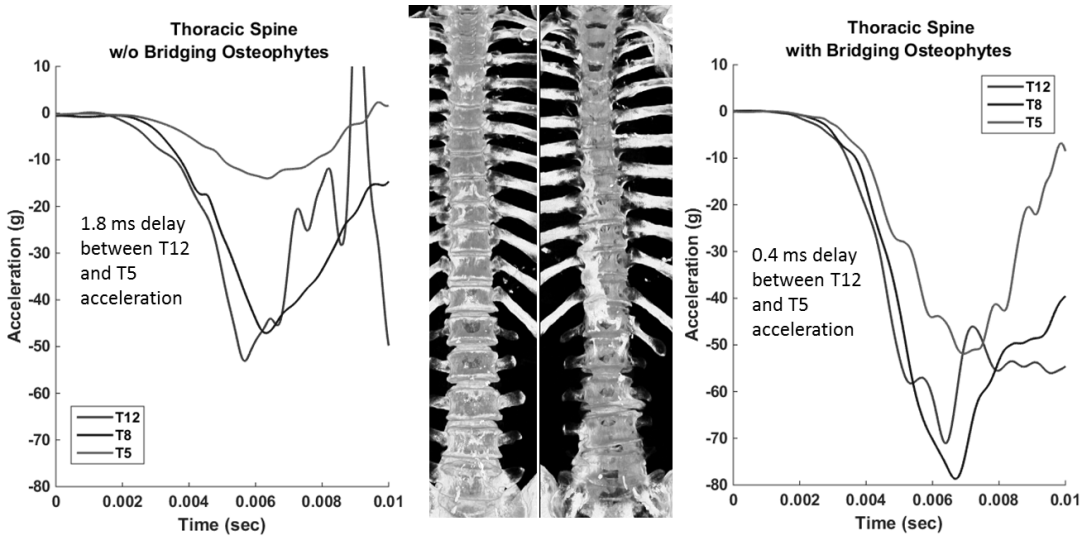

Fig. 13. Observation of the effect of bridging osteophytes: (left) Spine without osteophytes shows a 1.8 ms phasing between onset at T5 relative to T12, (right) Spine with bridging osteophytes from T12 to T6 shows a 0.4 ms (80% reduction) phasing between onset at T5 relative to T12

5.3 Spinal Kinematics

The rotational behavior of the spine showed similar trends to what was expected due to the anatomy. The sacrum showed the highest degree of rotation with a consistent posterior rotation of 6.7 ± 1.7°. In one instance, the seat loading preceded floor loading by >2 ms which resulted in the sacrum going into anterior rotation. Other than T1 all other vertebral bodies went into a positive rotation about the Y-axis with minimal rotation in the X and Z axes. A representative rotational response of the spine is shown in Figure 14.

In addition to the individual rotational behavior of the spine, the relative rotation across each spine segment was calculated. Segmental rotations were calculated by evaluating the difference between the rotation of the superior vertebral body of the segment relative to the inferior vertebral body. For example, the L3-S1 segment showing a negative rotation indicates the relative angle between L3 and S1 was decreasing. The maximum relative rotation was seen in the

lumbar and upper thoracic spine. The thoracolumbar region, T12-L3 and T8-T12, showed the lowest level of relative rotation across the segments.

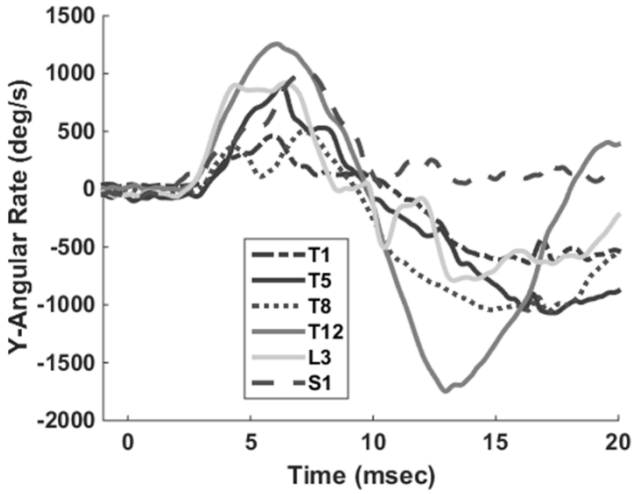

Fig. 14. Characteristic spinal angular rate response at Condition A (low severity)

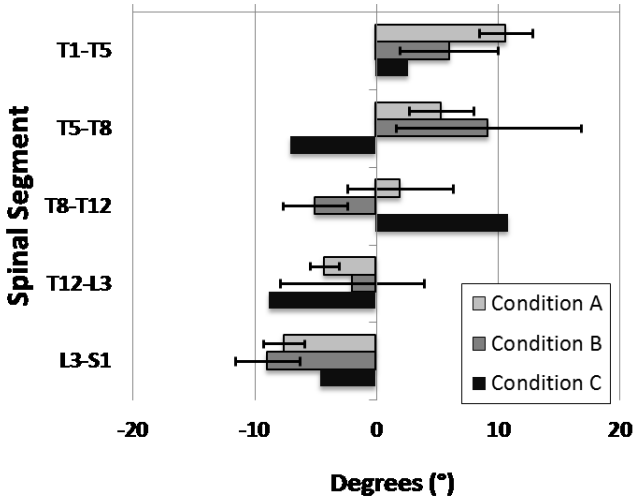

Fig. 15. Relative spinal segment rotation between upper and lower vertebral bodies. Condition C (severe case) sustained a vertebral body fracture at T12 prior to peak rotation.

5.4 CT Bone Density

Vertebrae L5 to T5 were analyzed to compute mean body HU intensities from the CT scans of the twelve specimens. (Table 3) After each specimen was tested, a licensed medical examiner evaluated each PMHS specimen for vertebral body fractures (boxed values) by both CT and anatomical dissection.

A one-tailed t-test was conducted between the mean HU intensities of the six fractured vertebral bodies and those of the remaining bodies to test the hypothesis that the mean of the population of all fractured bodies is less than that of the non-injured bodies. A significant p-value ($p < 0.05$) resulted from the test. Additionally, a two-tailed t-test was conducted between the mean HU intensities of the fractured vertebral bodies from T5 to T10 and the intensities of those fractured from T11 to L5. A significant p-value ($p < 0.05$) resulted from the test.

Table 3. Summary of mean HU values for each vertebral body analyzed within each tested specimen. The gradient from light to dark indicates decreasing HU values relative to the set. Boxed values are vertebral bodies that sustained injuries during testing.

Vertebral Body	Specimen # 1	2	3	4	5	6	7	8	9	10	11	12
L5	185	114	142	149	107	153	126	175	123	157	86	**118**
L4	173	146	99	136	**91**	142	119	164	115	144	97	109
L3	175	120	89	152	85	125	117	154	107	149	**94**	96
L2	145	106	90	143	85	130	118	144	102	133	84	111
L1	130	91	78	118	85	113	122	145	112	87	89	105
T12	118	172	112	123	104	109	131	163	116	**96**	106	102
T11	121	140	126	142	136	115	132	165	132	91	128	115
T10	168	123	107	147	162	116	133	161	137	133	123	127
T9	167	200	110	138	109	128	116	149	133	118	122	131
T8	122	191	96	139	89	123	131	181	130	144	147	114
T7	136	189	100	164	142	112	131	190	133	157	143	122
T6	128	133	129	157	184	117	**133**	198	135	192	150	119
T5	167	144	105	178	239	118	116	217	137	200	**139**	123

6. Discussion

Four out of the seven tested PMHS yielded acceleration and angular velocity response data along the length of the spine without sustaining a fracture along its primary load path. The measured spinal response peaked in the thoracolumbar region at L3 for condition B and C, and T12 for condition A. The sacrum acceleration was notably lower, 35% on average, than the L3 acceleration which was an unexpected result due to it being only joint connecting the pelvis to the lumbar spine. The cause of this phenomenon may be due to the fact that the measurement of the sacrum acceleration is being collected at a single point on its posterior aspect and this point acceleration does not accurately represent the inertial loading of the pelvis on the lumbar spine. The location of measurement is not coincident with the center of gravity of the pelvis and a rigid body assumption is improper due to the flexibility of the sacroiliac joint, the fibrous joints connecting the iliac wings to the sacrum. Acceleration and angular velocity sensors were added in later tests to record the behavior of the anterior portion of the pelvis, and though enough data was not collected to draw conclusive evidence, the accelerations at the ischial tuberosities were consistently higher than those recorded at the sacrum. The relative difference between the anterior loading and posterior loading of the pelvis may influence the low acceleration response recorded at the sacrum.

Three of the seven PMHS sustained compression fractures during testing. Two the three compression fractures created, one each at condition B and C, fell within the thoracolumbar region while the third, at T6 at condition B, was located atop a spinal column with bridging osteophytes from T12 to T6. (Figure 13) The thoracolumbar region, where epidemiological studies have shown compression and burst fractures to be most prevalent in UBB events from theater (Blair 2012), contained peak spinal accelerations coincident with minimal relative rotations of spinal segments. High acceleration in conjunction with minimal segmental rotation are in agreement with the behavior that has been shown to cause compression, burst, and wedge

fractures in spinal segments from component level testing (Storvik 2010, Yoganandan 2013). Alignment of the lumbar spine also contributes while seated, a more vertically aligned spinal column as opposed to the natural standing lordosis (Figure 1), increasing the load share handled by the vertebral body since less bending results in less loading of the facets (Shirazi-Adl 1987, Miller 1983).

The CT bone density measurements showed a significantly lower HU value for fractured bodies as compared to non-fractured bodies. HU values have been highly correlated to bone strength based on previous literature (Kopperdahl 2002, Schreiber 2011), so lower HU values should correspond to a higher risk of injury, which agrees with the results. However, the injured vertebral bodies were not the lowest HU value in their respective spines, or even the lowest value nearest the input, indicating that while bone density may have value in assessing risk of failure, it alone cannot be predictive of failure location within a spinal column.

This study is limited by a small sample size and narrow range of input conditions. Spinal accelerations were analyzed in their installed coordinate frame which, while having less than 10° sagittal angle difference on average, does not correspond to an anatomical frame or the defined global coordinate frame. Bone density measurements were not calibrated against a radiographic phantom, similar to Schrieber et al, however they were done using consistent parameters so relative differences across specimen within the current study are possible, but HU values should not be used for wider analysis.

The experimental model has shown to be repeatable and has yielded valuable results. This study is ongoing and is projected to increase the sample size while exploring the effect of both duration and magnitude of input velocity. Further analysis will analyze the spinal accelerations in a parallel coordinate frame so that a transfer function may be developed between input conditions and spinal response. Combination of Vicon, CT, and CMM data will be utilized to define

vertebral body initial positions to better understand the segmental rotations and spinal compression and their association with injury. The results of the current study and ongoing work can be used to more accurately define boundary conditions for component level spine testing.

7. Conclusions

Spinal accelerations and angular velocities were recorded at six levels along the lumbar and thoracic spine yielding non-injurious spinal acceleration and angular velocity data in four of seven PMHS tests. From the three specimen that sustained compression fractures, the following trends were observed:

- Peak spinal acceleration was observed in the thoracolumbar spinal region for all loading conditions. The peak loading did not consistently coincide with the location of the compressive fracture sustained.
- Relative segmental rotation was minimal in the region L3-T8, indicating that within this segment, the spinal column was axially aligned with the vertical loading vector. Previous literature supports that pure compression maximizes load on the vertebral body and reduces the load shared by the facet joints.
- Quantitative CT bone density analysis identified fractured vertebral bodies as having significantly lower relative densities than unfractured vertebral bodies. However, fractured vertebral bodies were not always the least dense body within a specimen or even the least body closest to the loading.

From these observations, while severity of loading, positioning, and bone density all influence the risk of vertebral compression fracture, none of those three factors are predictive of injury in isolation of the others. Further exploration on the influence of each of these factors to

injury risk may uncover a relationship allowing prediction, and eventually mitigation, of compression fracture in the vertical inertial loading environment.

Appendix A: Measured System and Spinal Responses

The following section contains all of the acceleration and angular rate responses from the system and spine that were included in the analysis.

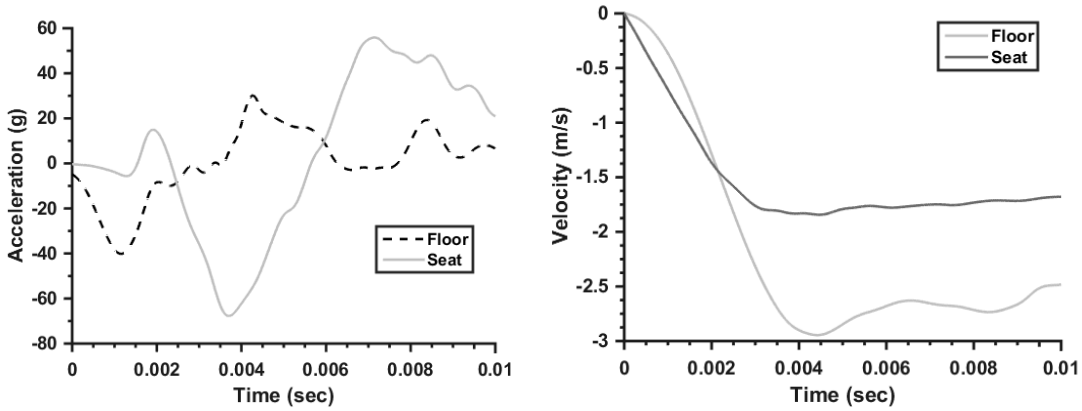

Figure A.1 System input acceleration and velocity for Condition A: Test 1

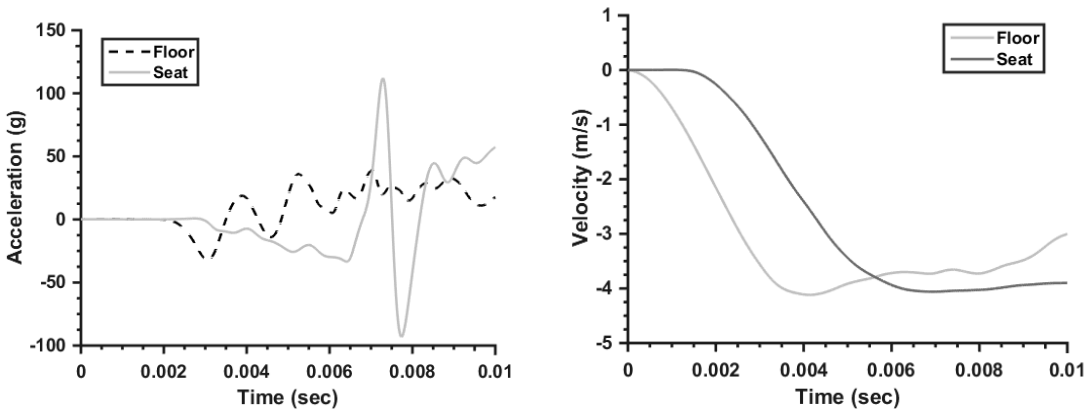

Figure A.2 System input acceleration and velocity for Condition A: Test 2

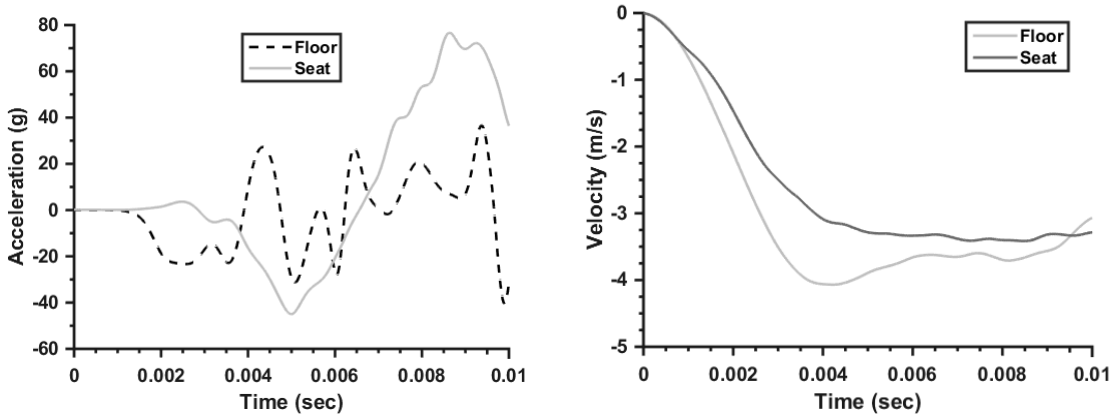

Figure A.3 System input acceleration and velocity for Condition A: Test 3

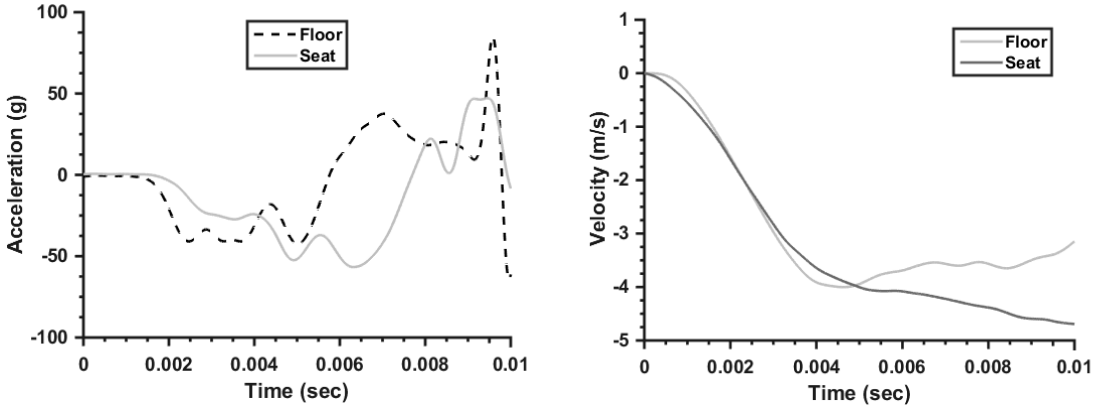

Figure A.4 System input acceleration and velocity for Condition A: Test 4

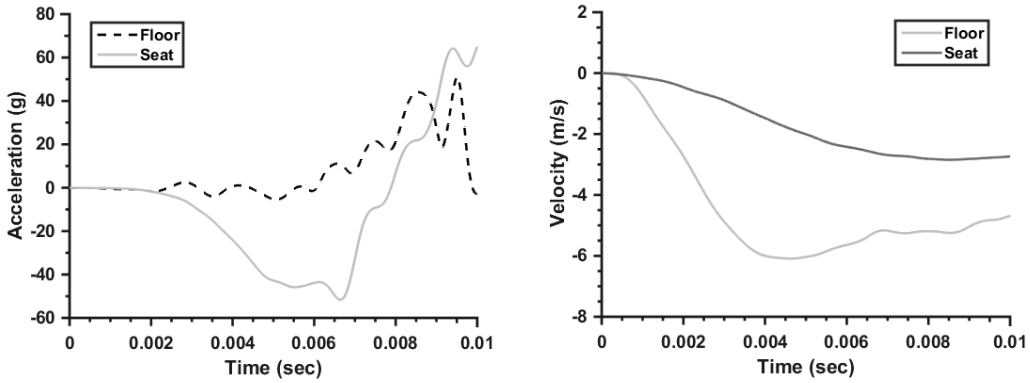

Figure A.5 System input acceleration and velocity for Condition B: Test 1

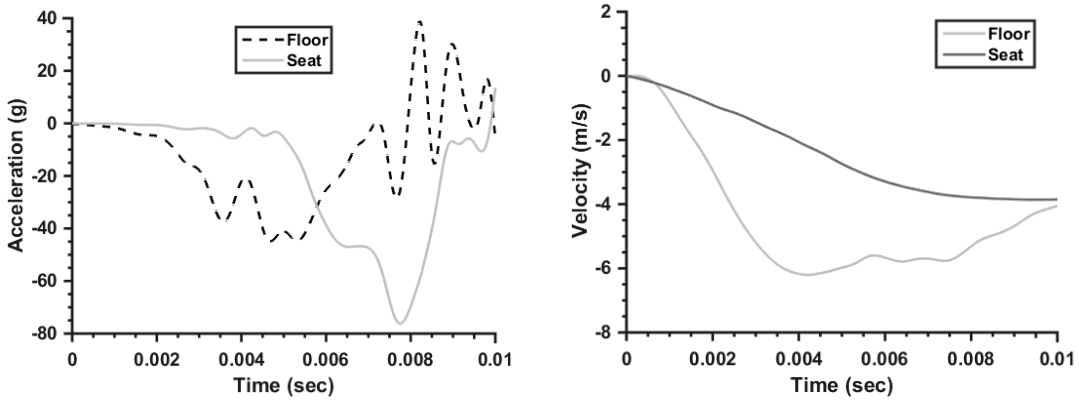

Figure A.6 System input acceleration and velocity for Condition B: Test 2

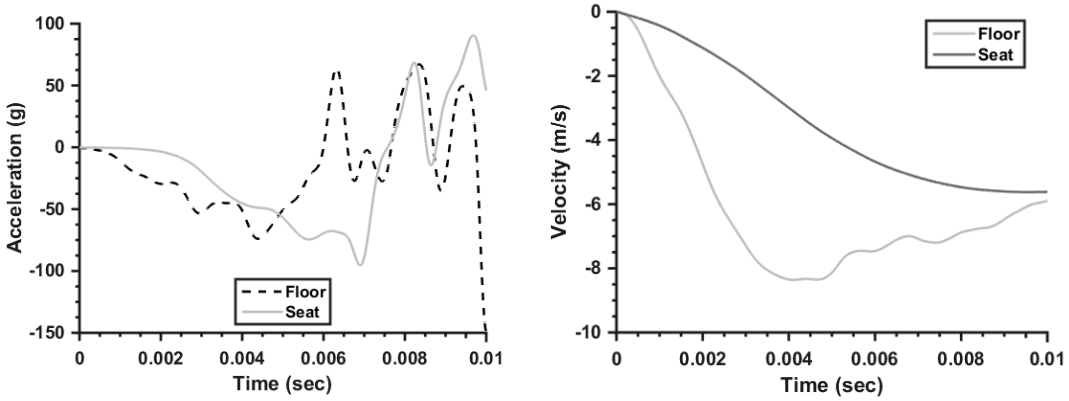

Figure A.7 System input acceleration and velocity for Condition C: Test 1

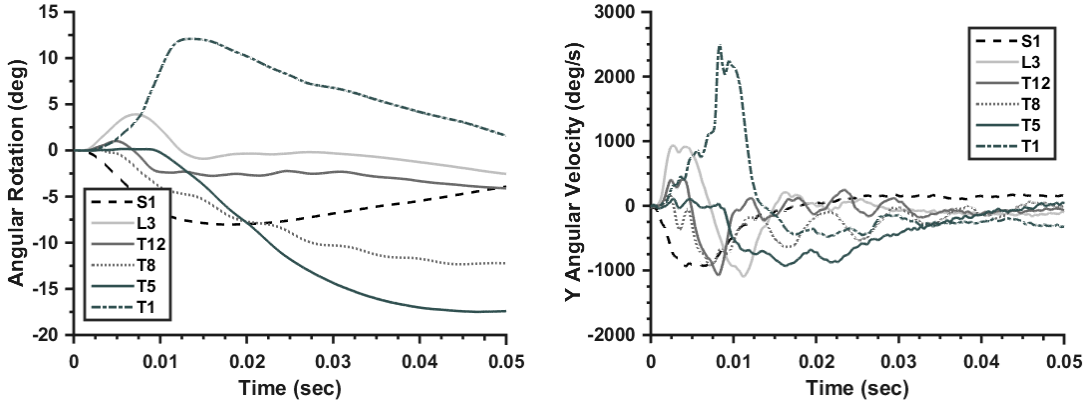

Figure A.8 Spinal angular rotation and velocity for Condition A: Test 1

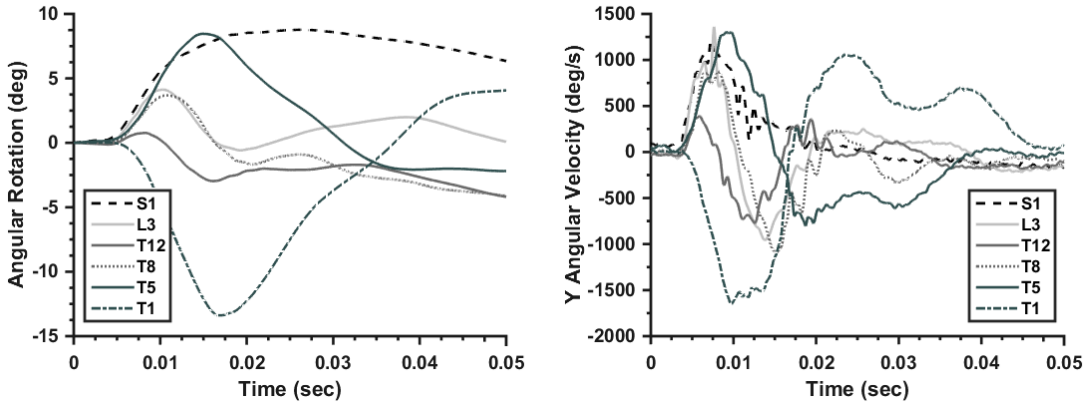

Figure A.9 Spinal angular rotation and velocity for Condition A: Test 2

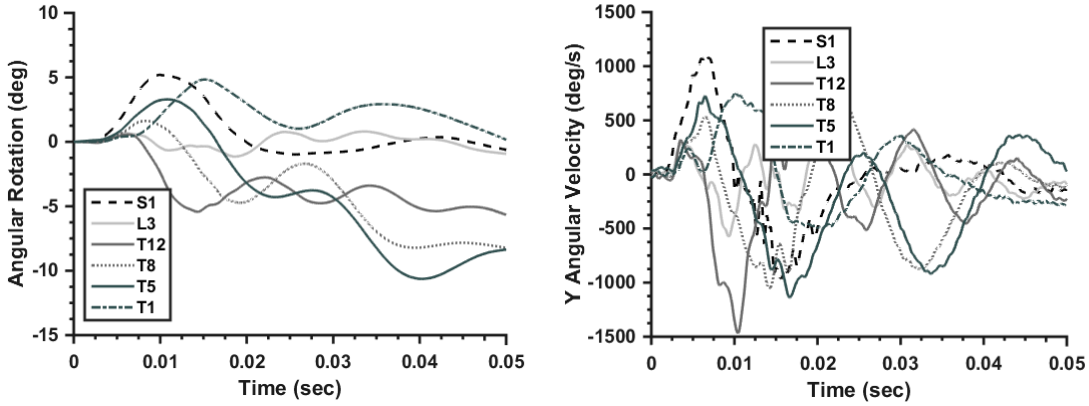

Figure A.10 Spinal angular rotation and velocity for Condition A: Test 3

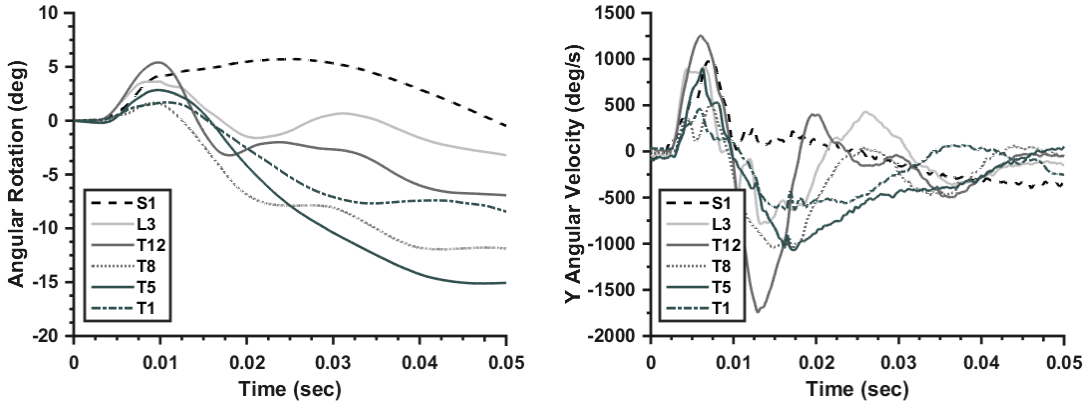

Figure A.11 Spinal angular rotation and velocity for Condition A: Test 4

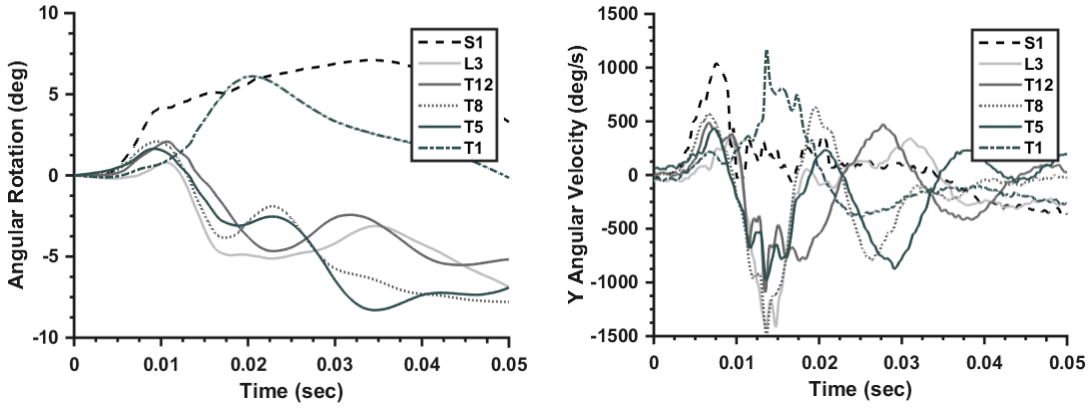

Figure A.12 Spinal angular rotation and velocity for Condition B: Test 1

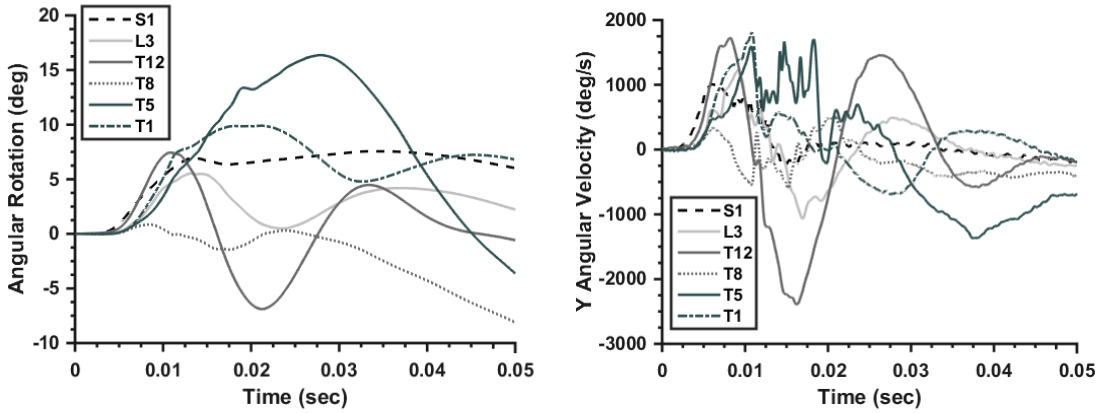

Figure A.13 Spinal angular rotation and velocity for Condition B: Test 2

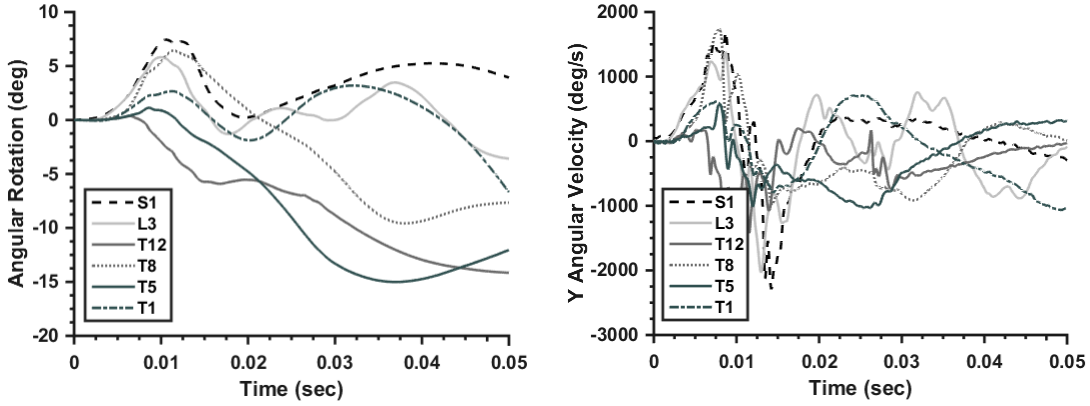

Figure A.14 Spinal angular rotation and velocity for Condition C: Test 1

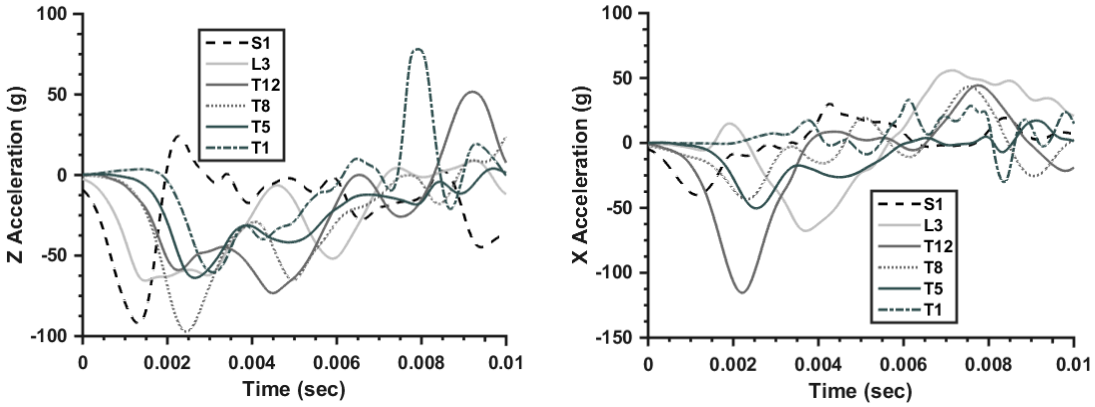

Figure A.15 Spinal sagittal acceleration responses (X and Z) for Condition A: Test 1

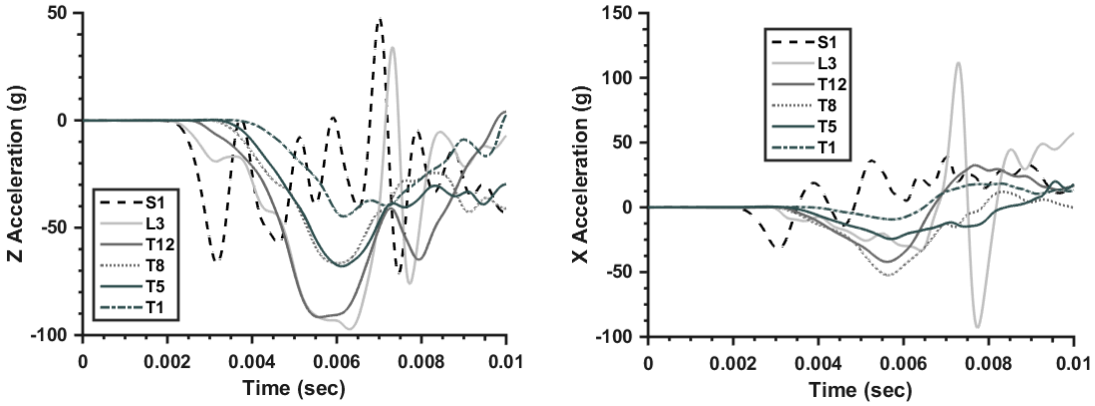

Figure A.16 Spinal sagittal acceleration responses (X and Z) for Condition A: Test 2

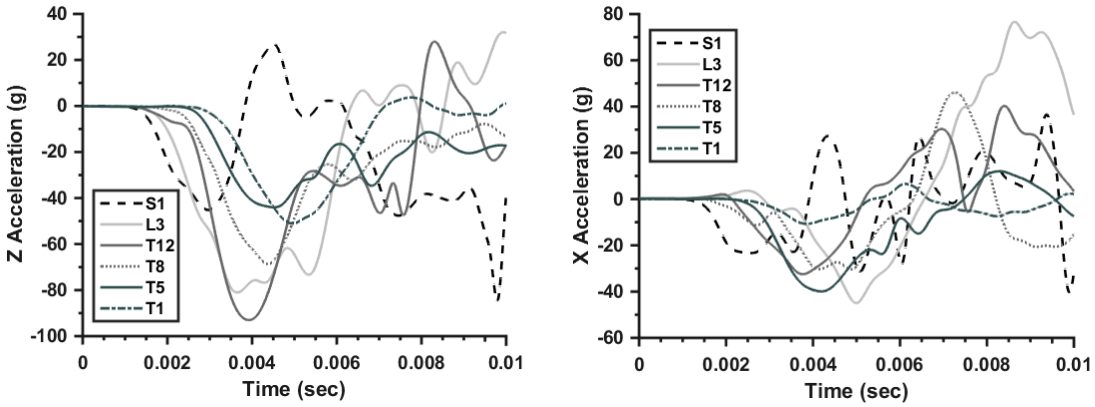

Figure A.17 Spinal sagittal acceleration responses (X and Z) for Condition A: Test 3

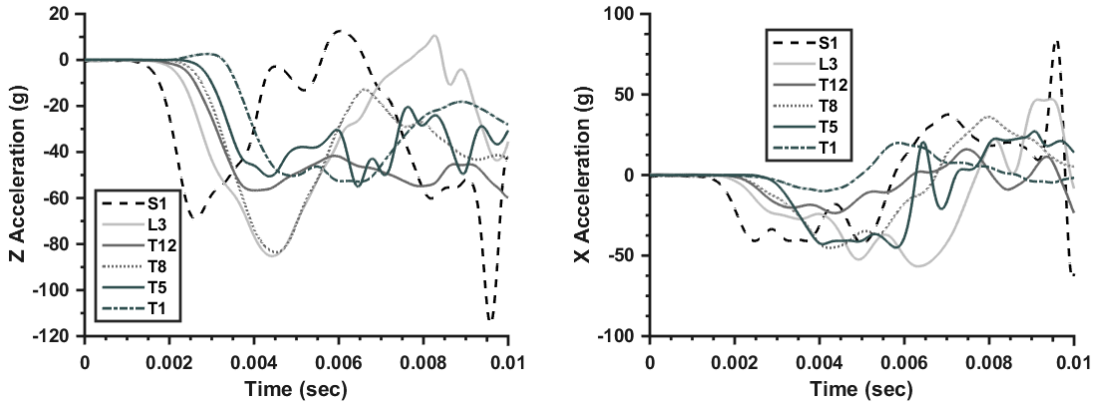

Figure A.18 Spinal sagittal acceleration responses (X and Z) for Condition A: Test 4

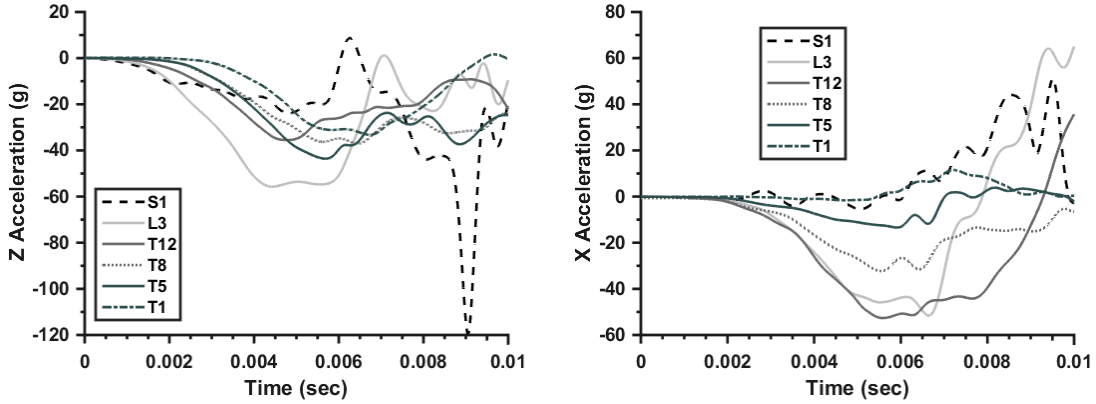

Figure A.19 Spinal sagittal acceleration responses (X and Z) for Condition B: Test 1

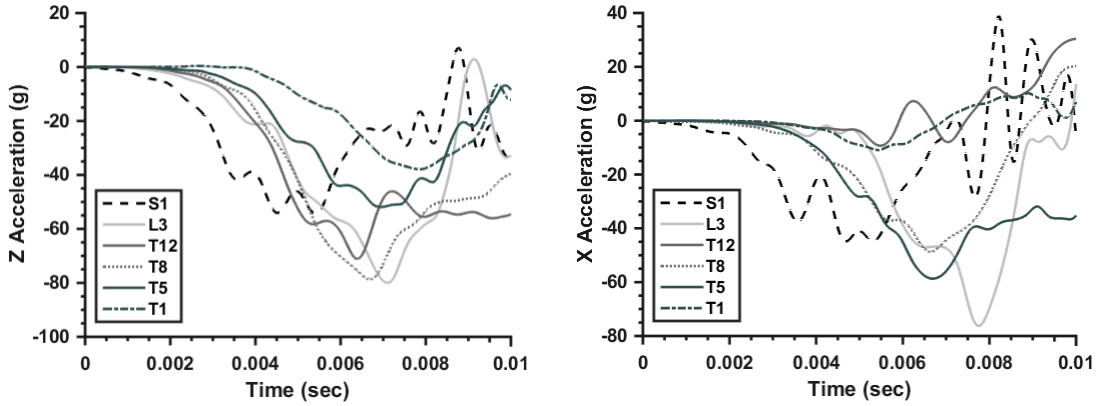

Figure A.20 Spinal sagittal acceleration responses (X and Z) for Condition B: Test 2

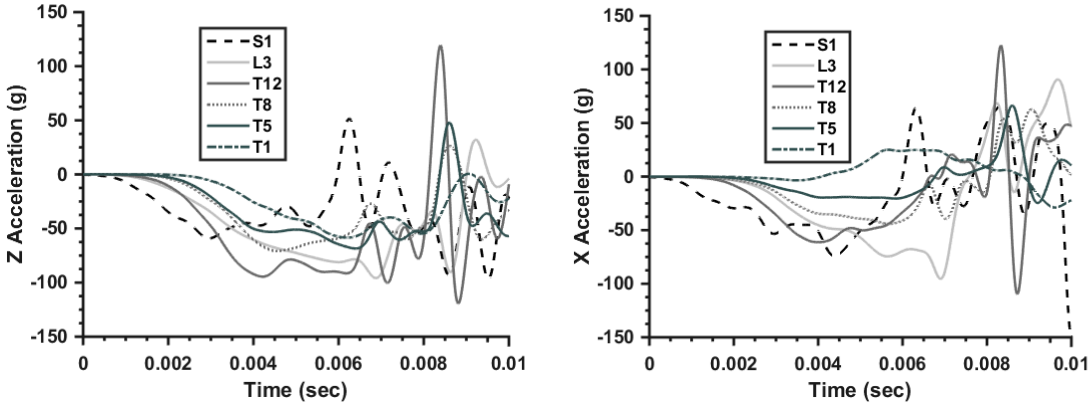

Figure A.21 Spinal sagittal acceleration responses (X and Z) for Condition C: Test 1

Bibliography

Allsop D, Perl T, and Warner C. Force/deflection and fracture characteristics of the temporo-parietal region of the human head. Proceedings of the 35th Stapp Car Crash Conference, SAE Paper No. 912907, 1991.

Arepally, Sudhakar, et al. Application of mathematical modeling in potentially survivable blast threats in military vehicles. No. TARDEC-19214RC. ARMY TANK-AUTOMOTIVE RESEARCH AND DEVELOPMENT CENTER WARREN MI, 2008.

Bailey, Ann M., et al. "Comparison of Hybrid-III and PMHS response to simulated underbody blast loading conditions." *Proceedings of IRCOBI Conference*. 2013.

Belkoff, Stephen M., et al. "The biomechanics of vertebroplasty: the effect of cement volume on mechanical behavior." *Spine* 26.14 (2001): 1537-1541.

Blair, James A., et al. "Military penetrating spine injuries compared with blunt." The Spine Journal 12.9 (2012): 762-768.

Christiansen, Blaine A., et al. "Mechanical contributions of the cortical and trabecular compartments contribute to differences in age-related changes in vertebral body strength in men and women assessed by QCT-based finite element analysis." *Journal of Bone and Mineral Research* 26.5 (2011): 974-983.

Cormier J, Manoogian S, Bisplinghoff J, McNally C, and Duma S. The use of acoustic emission in facial fracture detection. Biomed Sci Instrum, vol. 44, pp. 147-152, 2008.

Denis, Francis. "The three column spine and its significance in the classification of acute thoracolumbar spinal injuries." spine 8.8 (1983): 817-831.

Dooley, C. J., et al. "Response of thoracolumbar vertebral bodies to high rate compressive loading-biomed 2013." Biomedical sciences instrumentation 49 (2012): 172-179.

Edwards, W. Thomas, et al. "Structural features and thickness of the vertebral cortex in the thoracolumbar spine." Spine 26.2 (2001): 218-225.

Eswaran, Senthil K., et al. "Cortical and trabecular load sharing in the human vertebral body." *Journal of Bone and Mineral Research* 21.2 (2006): 307-314.

Ewing, Channing L., Albert I. King, and Priyaranjan Prasad. "Structural considerations of the human vertebral column under+ gz impact acceleration." *Journal of Aircraft* 9.1 (1972): 84-90.

Funk JR, Crandall JR, Tourret LJ, MacMahon CB, Bass CR, Patrie JT, Khaewpong N, and Eppinger RH. The axial injury tolerance of the human foot/ankle complex and the effect of Achilles tension. Journal of Biomechanical Engineering, vol. 124(6), pp. 1-8, 2002.

Glaister, D. H. "The effects of acceleration of short duration." *A Textbook of Aviation Physiology*. Pergamon Press Oxford, 1965. 746-794.

Gondusky, Joseph S., and Michael P. Reiter. "Protecting military convoys in Iraq: an examination of battle injuries sustained by a mechanized battalion during Operation Iraqi Freedom II." Military medicine 170.6 (2005): 546-549.

Gowdy, Van, et al. A lumbar spine modification to the Hybrid III ATD for aircraft seat tests. No. 1999-01-1609. SAE Technical Paper, 1999.

Base, Wright-Patterson Air Force. "Biomechanics of the Vertebral Column and Internal Organ Response to Seated Spinal Impact in the Rhesus Monkey (Macaca Mulatta) 1 LE Kazarian, JW Hahn, 2 and HE von Gierke Aerospace Medical Research Laboratory." *Proceedings of... Stapp Car Crash Conference*. Vol. 14. No. 544. The Society, 1970.

King, A.I. “Biomechanics of the spine and pelvis.” SAE Paper No. 730413, pp. 55-67, 1973

Kopperdahl, David L., Elise F. Morgan, and Tony M. Keaveny. "Quantitative computed tomography estimates of the mechanical properties of human vertebral trabecular bone." *Journal of orthopaedic research* 20.4 (2002): 801-805.

Langrana, N. A., et al. "Acute thoracolumbar burst fractures: a new view of loading mechanisms." *Spine* 27.5 (2002): 498-508.

Lu, Yongtao, et al. "Strain changes on the cortical shell of vertebral bodies due to spine ageing: A parametric study using a finite element model evaluated by strain measurements." *Proceedings of the Institution of Mechanical Engineers, Part H: Journal of Engineering in Medicine* 227.12 (2013): 1265-1274.

MacLean, Jeffrey J., Julia P. Owen, and James C. Iatridis. "Role of endplates in contributing to compression behaviors of motion segments and intervertebral discs." *Journal of biomechanics* 40.1 (2007): 55-63.

Michaelson, Jarett, et al. "Rear seat occupant safety: kinematics and injury of PMHS restrained by a standard 3-point belt in frontal crashes." Stapp car crash journal 52 (2008): 295-325.

Miller, J. A. A., K. A. Haderspeck, and A. B. Schultz. "Posterior element loads in lumbar motion segments." Spine 8.3 (1983): 331-337.

Owens, Brett D., et al. "Characterization of extremity wounds in operation Iraqi freedom and operation enduring freedom." Journal of orthopaedic trauma 21.4 (2007): 254-257.

Oxland, Thomas R., et al. "Effects of endplate removal on the structural properties of the lower lumbar vertebral bodies." *Spine* 28.8 (2003): 771-777.

Patwardhan, Avinash G., et al. "A Follower Load Increases the Load-Carrying Capacity of the Lumbar Spine in Compression." *Spine* 24.10 (1999): 1003-1009.

Petitjean, Audrey, et al. "Laboratory Reconstructions of Real World Frontal Crash Configurations using the Hybrid III and THOR Dummies and PMHS." Stapp car crash journal 46 (2002): 27-54.

Pintar FA, Yoganandan N, Stemper BD, Bostrom O, Rouhana SW, Digges KH, and Fildes BN. Comparison of PMHS, World SID, and THOR-NT responses in simulated far side impact. Stapp Car Crash Journal, vol. 51, pp. 313-360, 2007.

Possley, D.R., et al., The effect of vehicle protection on spine injuries in military conflict. The Spine Journal, 2012. 12(9): p. 843-848.

Polanco, Michael A., and Justin D. Littell. "Vertical Drop Testing and Simulation of Anthropomorphic Test Devices." (2011).

Ragel, B.T., et al., Fractures of the thoracolumbar spine sustained by soldiers in vehicles attacked by improvised explosive devices. Spine, 2009. 34(22): p. 2400-2405.

Ramasamy, Arul, et al. "Injuries from roadside improvised explosive devices." Journal of Trauma and Acute Care Surgery 65.4 (2008): 910-914.

Reed, Matthew P., and Sheila M. Ebert. "The seated soldier study: posture and body shape in vehicle seats." (2013).

SAE, J. "J211-1 Instrumentation for Impact Test—Part 1—Electronic Instrumentation." Society of Automotive Engineers, Warrendale PA (2003).

Salzar, R.S., et al., Ejection injury to the spine in small aviators: sled tests of manikins vs. post mortem specimens. Aviation, space, and environmental medicine, 2009. 80(7): p. 621-628.

Schindelin, Johannes, et al. "Fiji: an open-source platform for biological-image analysis." *Nature methods* 9.7 (2012): 676-682.

Schneider, Caroline A., Wayne S. Rasband, and Kevin W. Eliceiri. "NIH Image to ImageJ: 25 years of image analysis." *Nature methods* 9.7 (2012): 671-675.

Schreiber, Joseph J., et al. "Hounsfield units for assessing bone mineral density and strength: a tool for osteoporosis management." *The Journal of Bone & Joint Surgery* 93.11 (2011): 1057-1063.

Shirazi-Adl, A., and G. Drouin. "Load-bearing role of facets in a lumbar segment under sagittal plane loadings." Journal of biomechanics 20.6 (1987): 601-613.

Silva, Matthew J., Tony M. Keaveny, and Wilson C. Hayes. "Load sharing between the shell and centrum in the lumbar vertebral body." *Spine* 22.2 (1997): 140-150.

Stapp, J. P. "Jolt effects of impact on man." *Impact Acceleration Stress: Proceedings of a Symposium. Washington DC: National Academy of Sciences-National Research Council, Publication*. Vol. 977. 1962.

Stapp, John Paul. "Human tolerance to deceleration; summary of 166 runs." *Journal of aviation medicine* 22.1 (1951): 42-5.

Stemper, Brian D., et al. "A new PMHS model for lumbar spine injuries during vertical acceleration." Journal of biomechanical engineering 133.8 (2011): 081002.

Stemper, B., et al. Loading Rate Dependency of Thoraco-Lumbar Spine Fracture Location: An Investigation of Trauma in Military Scenarios. in Disorders of the Spine and Peripheral Nerves. 2012. Orlando, Florid.

Stemper, Brian D., et al. "Rate-dependent fracture characteristics of lumbar vertebral bodies." *Journal of the mechanical behavior of biomedical materials* 41 (2015): 271-279.

Storvik, Steven G., et al. "Experimental Induction of Lumbar Spine Compression-Flexion Injuries." ASME 2010 Summer Bioengineering Conference. American Society of Mechanical Engineers, 2010.

Stumpf, Bill, Don Chadwick, and Bill Dowell. "The kinematics of sitting." Herman Miller, Zeeland, MI. Pamphlet (1995).

van der Veen, Albert J., et al. "Contribution of verftebral bodies, endplates, and intervertebral discs to the compression creep of spinal motion segments." *Journal of biomechanics* 41.6 (2008): 1260-1268.

Van Toen, C., et al. "Acoustic emission signals can discriminate between compressive bone fractures and tensile ligament injuries in the spine during dynamic loading." Journal of biomechanics 45.9 (2012): 1643-1649.

Vulcan, A. P., Albert I. King, and G. S. Nakamura. "Effects of bending on the vertebral column during+ Gz acceleration." *Aerospace medicine* 41.3 (1970): 294-300.

Yoganandan, Narayan, et al. "Biomechanics of human thoracolumbar spinal column trauma from vertical impact loading." Annals of advances in automotive medicine 57 (2013): 155.

Zhang, JiangYue, et al. *A High-Fidelity Model for Lumbar Spine Injury Investigation during Under Body Blast Loading*. RTO-MP-HFM-207-A Survey of Blast Injury across the Full Landscape of Military ScienceNATO: Halifax, CANADA, 2011.

Zhang, JiangYue, et al. "Effects of Torso-Borne Mass and Loading Severity on Early Response of the Lumbar Spine under High-Rate Vertical Loading."

Curriculum Vitae

Christopher J. Dooley

24 S Decker Ave, Baltimore, MD 21224
chris.dooley5@gmail.com
(513) 703-5761

Work Experience

Johns Hopkins University Applied Physics Lab
Biomechanical Engineer
Baltimore, MD
06.2011 – 09.2011, 06.2012 – Present
Involved with development and implementation of test protocols and instrumentation planning for tissue, component, and whole body PMHS testing. Data analysis and presentation to sponsors and wider community. Strategic planning for future work and areas of research.

The Ohio State University Injury Biomechanics Research Laboratory
Research Assistant
Columbus, OH
10.2011 – 06.2012
Involved in specimen preparation and test execution for multiple types of PMHS and ATD automotive crash testing and component level tissue testing.

Education

Johns Hopkins University - Whiting School of Engineering
Baltimore, MD
M.S. Mechanical Engineering
01.2013 – Present

The Ohio State University - Dept. of Biomedical Engineering
Columbus, OH
B.S. Biomedical Engineering with Honors Research Distinction
Minor in Business
09.2008 – 06.2012
Thesis Topic: Stiffness determination techniques for determination of differences between oblique and lateral automotive impacts

Publications

Dooley, C. J., et al. "Response of thoracolumbar vertebral bodies to high rate compressive loading-biomed 2013." Biomedical sciences instrumentation 49 (2012): 172-179.

Dooley, Chris. "Analysis of Stiffness Calculation Methods for Biomechanical Testing when Loading and Measurement are not Coincident Spatially." The Ohio State University (2012). http://hdl.handle.net/1811/51841

Awards

JHU/APL Research and Exploratory Development Award for Excellence and Dedication (10.2015)

JHU/APL Special Achievement Award (08.2014)
Given for going above and beyond work requirements in the high quality execution of critical sponsor tests on a shortened time frame.

Biomedical Engineering Undergraduate Service Award (06.2012)
OSU BME Senior showing dedication to service for the department and the community

References

Available on request.